nature communications

Article

https://doi.org/10.1038/s41467-025-60694-5

Production of live monkeys and their genetically matched embryonic stem cells from single embryos

Received: 24 November 2024

Accepted: 27 May 2025

Published online: 01 July 2025

Check for updates

Chenyang Si[1,2,5], Ran Zhu[1,2,3,5], Junmo Wu[1,2,5], Zhenzhen Chen[1,2,5], Zengli Tang[1,3], Zuoyao Li[1], Yu Kang[1,2], Lifeng Xiang[4], Jiawei Zuo[1,3], Pengpeng Yang[1,2], Chu Chu[1,2], Shanshan Yang[1], Zifan Li[1,2], Lu Zhao[1,2], Xinglong Chen[1,2], Youwei Pu[1,2], Baohong Tian[1,2], Zhaohui Yang[1,2], Weizhi Ji[1,2] ✉, Shaoxing Dai[1,2] ✉ & Yuyu Niu[1,2] ✉

Immune rejection poses a challenge in stem cell therapy, especially with allogeneic embryonic stem cells (ESCs). Non-human primates offer a promising avenue for developing genetically matched ESCs for regenerative medicine. Here, we successfully derive three live monkeys and their genetically matched autologous ESCs (aESCs) using embryo splitting. Additionally, from fibroblasts of one of these monkeys, we generate induced pluripotent stem cells (iPSCs) and nuclear transfer embryonic stem cells (ntESCs), creating a set of genetically matched aESCs, iPSCs, and ntESCs. Single-cell RNA-seq analysis reveals that aESCs potentially exhibit reduced heterogeneity, lower transcriptional noise, and enhanced genomic stability compared to iPSCs and ntESCs. Furthermore, we successfully derive ESCs from human split embryos, highlighting the potential for obtaining human aESCs. Collectively, our study offers an avenue for establishing autologous pluripotent stem cells and provides the theoretical basis as well as research model for further application of aESCs in human regenerative medicine.

Embryonic stem cells (ESCs) and induced pluripotent stem cells (iPSCs) represent promising sources for cell-based therapies[1–3]. Genetically matched cells, such as iPSCs and nuclear transfer embryonic stem cells (ntESCs), carry reduced risk of tissue rejection and can be engineered to deliver or express therapeutic agents[4,5]. However, both cell types face significant safety concerns and technical limitations. The process of somatic cell reprogramming is associated with the risk of acquisition of undesired gene mutations, genomic imprinting, and incomplete reprogramming, all of which can affect the functionality and safety of the resulting iPSCs[2,6–8]. The derivation of ntESCs requires the use of oocytes, a significant ethical and practical barrier, and involves complex and inefficient techniques[5,9,10]. These challenges slow down progress in the development of therapeutic methods and hinder the application of both iPSCs and ntESCs.

Genetically matched ESCs remain of high scientific interest for regenerative medicine, but their derivation from non-human primates and humans poses technical and ethical challenges. Embryo splitting is a promising strategy to address these issues. This technique mimics the natural process of forming monozygotic twins by separating a single embryo into identical embryos during the cleavage and blastocyst stages. It has been successfully applied in veterinary medicine for over 30 years to generate monozygotic twins with favored genetic

[1]State Key Laboratory of Primate Biomedical Research; Institute of Primate Translational Medicine, Kunming University of Science and Technology, Kunming, Yunnan, China. [2]Yunnan Key Laboratory of Primate Biomedical Research, Kunming, Yunnan, China. [3]Southwest United Graduate School, Kunming, Yunnan, China. [4]Department of Reproductive Medicine, The First People's Hospital of Yunnan Province; The Affiliated Hospital of Kunming University of Science and Technology, Kunming, Yunnan, China. [5]These authors contributed equally: Chenyang Si, Ran Zhu, Junmo Wu, Zhenzhen Chen. ✉e-mail: wji@lpbr.cn; daisx@lpbr.cn; niuyy@lpbr.cn

characteristics in sheep, horses, goats, pigs, and cows[11–15]. However, twinning experiments in non-human primates have yielded poor outcomes[16–18], and data on human split embryos are limited[19–22], indicating the need for technical improvements and ethical considerations. Should such barriers be overcome, embryo splitting technology might be applied in studies of reproductive biology and disease, to treat infertility and for embryo donations if ethically permitted.

ESC lines have also been successfully derived from single blastomeres in mice and humans, but this method has the limited efficiency and incomplete characterization[23–26]. Currently, blastocyst-derivation of ESCs remains the most effective method[27], with various pluripotent states reported, including primed[28], naïve[29], and other distinct pluripotent states[30,31]. However, it remains unclear whether ESCs can be derived from blastocysts of split embryos in monkeys, and what their characteristics would be.

To extend the boundaries of our knowledge about the developmental potential of the early embryo, we here set out to establish a method for embryo splitting. Through this technological advancement, we derived primate autologous ESCs (aESCs) and successfully derived ESCs from human split embryos. We also derived iPSCs and ntESCs from fibroblasts harvested from a newborn monkey, thereby establishing the non-human primate genetically matched ESCs, iPSCs, and ntESCs (Fig. 1a). Using single-cell RNA sequencing (scRNA-seq) analysis, we reveal that aESCs and ntESCs show less heterogeneity in differentiation potential on a feeder layer than iPSCs, with feeder-free culture conditions effectively reducing this heterogeneity. Notably, aESCs potentially maintain better genomic stability and display lower levels of transcriptional noise than iPSCs and ntESCs.

Results

Monkey split embryos show normal developmental potential in vitro

In this study, we used healthy 4-cell and 8-cell stage monkey embryos obtained via intracytoplasmic sperm injection for embryo splitting experiments. Specifically, we symmetrically split a total of 95 cynomolgus and 38 rhesus monkey 4-cell stage embryos. However, seven cynomolgus and two rhesus monkey 4-cell stage embryos experienced single or more blastomere breakages due to enzymatic or mechanical damage. Consequently, we successfully reconstituted 176 cynomolgus and 72 rhesus monkey 2/4th embryos (Supplementary Fig. 1a). Among these, 93 (53%) cynomolgus monkey and 33 (46%) rhesus monkey split embryos developed to the blastocyst stage. Of these, 56 cynomolgus (28 pairs, 60%) and 22 rhesus (11 pairs, 67%) were identical split embryos. We also used 8-cell stage embryos to conduct asymmetric embryo splitting (3/8 and 5/8, respectively) (Supplementary Fig. 1b and Supplementary Movie 1). In all, we successfully split eighty-one 8-cell embryos (46 cynomolgus and 35 rhesus monkeys), resulting in a total of 162 split embryos (92 cynomolgus and 70 rhesus monkeys). Of these, we detected successful progression to the blastocyst stage in forty-four 3/8th embryos (22 cynomolgus, 48% and 22 rhesus monkeys, 63%) and fifty-four 5/8th embryos (31 cynomolgus, 67% and 23 rhesus monkeys, 66%). Within this cohort, 40 cynomolgus monkey (20 pairs, 43%) and 42 rhesus monkey (21 pairs, 60%) were identical split embryos. Split embryos were no different from normal embryos in terms of developmental time, morphology (Fig. 1b, c), and blastocyst rate (Fig. 1g, h, Supplementary Fig. 1e, f), irrespective of whether symmetric or asymmetric embryo splitting was employed. The rate in which pairs of 8-cell split embryos developed into blastocysts resembled the normal embryo developmental rate (47.7%) (Fig. 1h and Supplementary Fig. 1f) but was lower in pairs of 4-cell split embryos (30.2%) (Fig. 1g and Supplementary Fig. 1e). This may be because division at the 8-cell stage prevents selecting only developmentally restricted vegetal blastomeres[32]. However, it remains unclear whether a similar phenomenon occurs in monkeys. Additionally, the inherent heterogeneity among blastomeres may also play a role in these observed differences[33–36].

To evaluate the developmental potential of split in vitro-cultured embryos, we investigated the expression patterns of the lineage-specific markers OCT4 (epiblast, Epi), CDX2 (trophoblast), and GATA6 (hypoblast, Hypo) in preimplantation and post-implantation stages. At day 6–10 post-fertilization (d.p.f. 6–10), the developmental morphology of split embryos was similar to controls (Fig. 1d), as evidenced by formation of the inner cell mass (ICM), marked by OCT4 at d.p.f.8 (Fig. 1e, f), and normal expression patterns of lineage-specific markers (Supplementary Fig. 1c, d)[37]. However, the total number of Epi and Hypo cells, as well as the number of Epi cells alone in split embryos at d.p.f.8, were significantly lower than those in controls (Fig. 1i, j, Supplementary Fig. 1j, l). Notably, we observed larger variations in numbers of Epi cells (12–51) and Hypo cells (11–74) in split embryos than in controls (Supplementary Fig. 1g, h). Moreover, the number of Epi cells differed between genetically matched split embryos at d.p.f.8 (Fig. 1i, j). However, we did not observe any significant differences in the number of Hypo cells between genetically matched 2/4th embryos (Supplementary Fig. 1i). In contrast, the number of Hypo cells in 3/8th embryos was significantly lower compared to 5/8th embryos at d.p.f.8 (Supplementary Fig. 1k). When comparing the Epi cell number in split embryos at d.p.f.8, we found that 5/8th embryos have comparable Epi cell counts to 2/4th embryos with higher Epi cell numbers, while 3/8th embryos have similar Epi cell counts to 2/4th embryos with lower Epi cell numbers (Fig. 1k).

In summary, our data support that the blastocyst rate, developmental timeline, and expression patterns of lineage-specific markers were comparable between split embryos and control embryos during d.p.f.6–10. However, the cell numbers of both Epi and Hypo were significantly lower in split embryos.

Establishment of ESCs and generation of live monkeys from split embryos

To explore the feasibility of deriving ESCs from split blastocysts in monkeys, we assessed a total of 25 2/4th blastocysts and twenty-six 3/8th blastocysts, and derived ESCs following established protocols[30,38]. Among these, twelve 2/4th blastocysts and thirteen 3/8th blastocysts formed ICM outgrowths, which gave rise to a total of 25 ESC lines (49%) (Fig. 2a and Supplementary Fig. 2d). Relative to controls, there were no differences in the efficiency of blastocyst attachment and ESC derivation (Fig. 2b, c). In ESCs derived from split blastocysts, dubbed spESCs, we observed a normal karyotype in three examined cell lines after 15 or more passages (Fig. 2f and Supplementary Fig. 2c). The spESC lines expressed pluripotency markers (OCT4, SOX2, and NANOG) (Fig. 2d, Supplementary Fig. 2a, and 2e) and differentiated into the three germ layers in vivo when injected into severe combined immune deficiency (SCID) mice (Fig. 2e and Supplementary Fig. 2b). To gain insight into the transcriptomes of spESCs, we conducted bulk RNA-sequencing (RNA-seq) analyses of 3 spESC and 3 ESC lines derived from control blastocysts. To ensure data reliability, we also analyzed publicly available RNA-seq datasets from cynomolgus monkey primed ESCs[39]. Notably, we found that the expression levels of pluripotency-related genes[40,41] were similar between spESCs and ESCs (Fig. 2g). Furthermore, in correlation analysis of gene expression patterns, we observed a strong correlation between spESCs and ESCs (Fig. 2h and Supplementary Fig. 2f). These results demonstrate that pluripotency characteristics, differentiation potential, and transcriptional signatures are highly similar between spESCs and ESCs derived from control blastocysts.

To assess the developmental potential of split embryos in vivo, we transferred 10 rhesus monkey 2/4th embryos into 5 rhesus monkey surrogates and 27 cynomolgus monkey 2/4th embryos into 16 cynomolgus monkey surrogates, respectively. Additionally, we transferred 9 thawed rhesus and 4 thawed cynomolgus monkey 5/8th embryos to corresponding surrogates (Fig. 3a). After 25 days, we confirmed pregnancy (11 singleton fetuses) by ultrasound examination in 3 rhesus and 8 cynomolgus monkey surrogates (Fig. 3b). The rates of pregnancy, implantation, and live birth were comparable between split and

https://doi.org/10.1038/s41467-025-60694-5

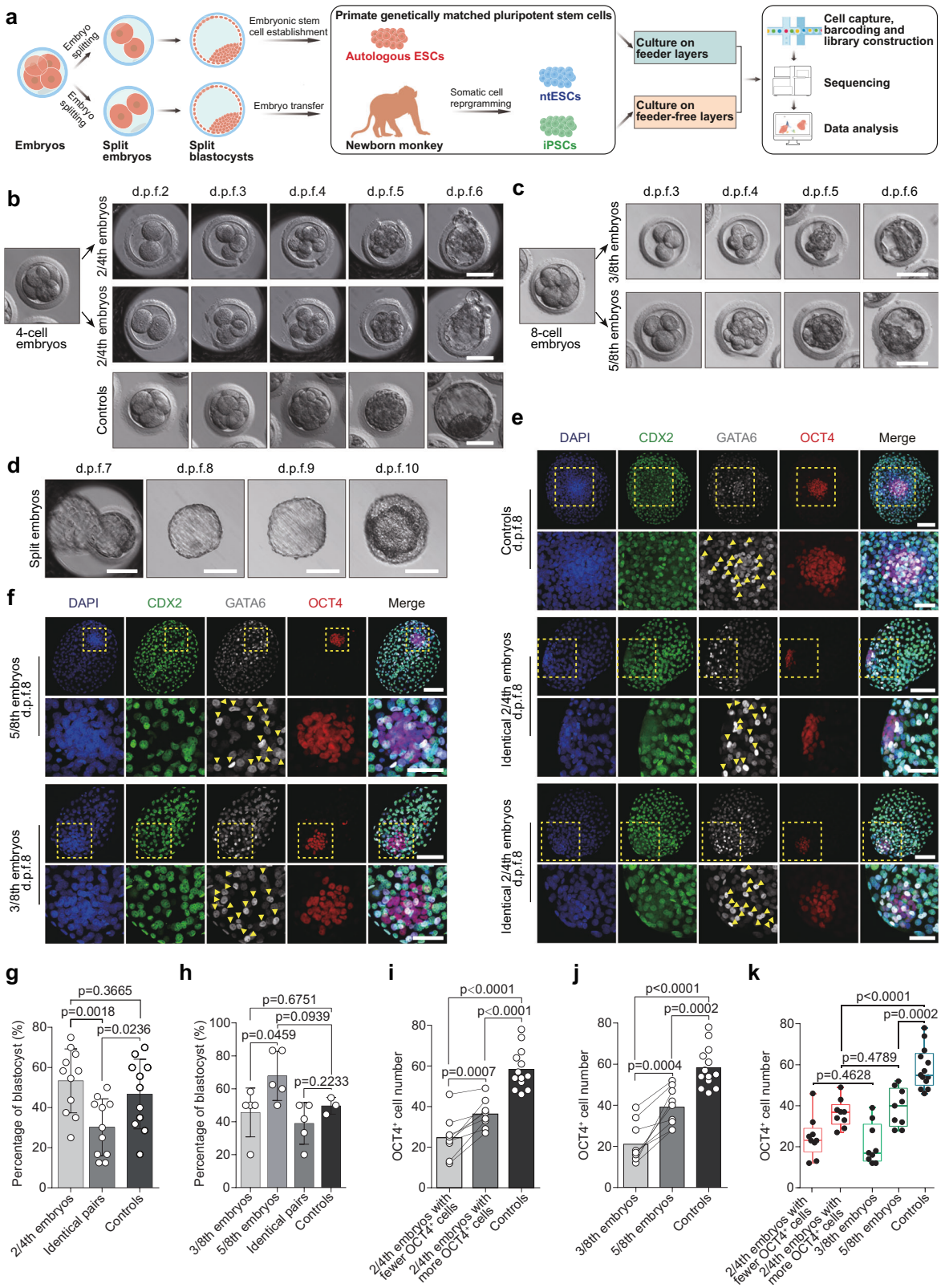

control embryos. (Fig. 3a). Nine offspring were successfully born. However, two cynomolgus pregnancies were aborted at 100 and 124 days of gestation (Supplementary Fig. 2h). Among the births, 6 babies were born by cesarean section at full term (3 females and 3 males) and others by natural labor (2 females and 1 male) (Supplementary Fig. 2h). In comparison with newborn monkeys obtained by transferring control embryos, we observed a normal growth rates in body weight and height in these monkeys (Fig. 3c, d). So far, 9 monkeys have survived and are growing healthily under human care. Among them, seven monkeys are four years old, while one is two years old and another one is more than one year old (Supplementary Fig. 2g).

In conclusion, these findings validate that split embryos have similar capacities to control embryos in establishing ESC lines and generating viable offspring.

Fig. 1 | Construction and in vitro development of split embryos. a Schematic diagram of the generation of aESCs and comparative analysis of genetically matched aESCs, iPSCs, and ntESCs. **b**, **c** Representative bright-field analysis of in vitro developmental progression showing that compaction and blastocyst cavity formation in split embryos occurs synchronously with that of control embryos. The 2/4th embryo refers to an embryo reconstructed from any two blastomeres of a 4-cell stage embryo. Similarly, the 5/8th and 3/8th embryos denote embryos reconstructed from any five blastomeres and the remaining three blastomeres of an 8-cell stage embryo, respectively. Similar results were obtained in no less than three independently repeated experiments. Scale bar, 100 μm. **d** Representative bright-field images of in vitro-split embryos developing from d.p.f.7 to d.p.f.10. Similar results were obtained in no less than three independently repeated experiments. **e**, **f** Identical split embryos and control embryos at d.p.f.8 were stained for lineage-specific markers (OCT4, CDX2, and GATA6). Yellow arrowheads represent Hypo cells (GATA6-positive, OCT4-negative, CDX2-negative). Scale bar, 100 μm. The scale bar in the magnified image represents 50 μm. **g** Percentage of 2/4th embryos that developed into blastocysts with a well-defined cavity at d.p.f.6 (cynomolgus monkey 2/4th embryos, n = 176; identical pairs, n = 56; controls, n = 169). Mean ± SEM presented for n = 11 independent experiments. Unpaired two-tailed Student's t-test. **h** Percentage of 3/8th and 5/8th embryos that developed into blastocysts. (cynomolgus monkey 3/8th and 5/8th embryos, n = 92; identical pairs, n = 40; controls, n = 53). The data for the split embryos and controls represent the mean of 5 and 3 independent experiments, respectively. Results are shown as mean ± SEM. The statistical analysis utilized the unpaired two-tailed Student's t-test. **i** Comparison of $OCT4^+$ cell numbers between genetically matched 2/4th embryos and control embryos at d.p.f.8. (2/4th embryos, n = 18, 9 pairs; controls, n = 13). Data from three independent experiments. Paired two-tailed Student's t-test without adjustment. **j** Comparison of $OCT4^+$ cell numbers between genetically matched 3/8th embryos and 5/8th embryos at d.p.f.8. (3/8th embryos and 5/8th embryos, n = 18, 9 pairs; controls, n = 13). Data from three independent experiments. The statistical analysis utilized the paired two-tailed Student's t-test without adjustment. **k** Comparison of $OCT4^+$ cell numbers among 2/4th embryos, 3/8th embryos, 5/8th embryos, and controls at d.p.f.8. Each dot represents one embryo for (**i**–**k**). (cynomolgus monkey 2/4th embryos, n = 18, 9 pairs; 3/8th embryos and 5/8th embryos, n = 18, 9 pairs; controls, n = 13). Data from three independent experiments are shown as mean ± SEM. The upper and lower edges of the box represent the maxima and minima, respectively, while the thick lines in the middle indicate the mean of each sample. The statistical analysis utilized the unpaired two-tailed Student's t-test without adjustment. Source data are provided as a Source Data file.

Derivation of autologous ESCs from split embryos

Prompted by the above findings, our next goal was to obtain a live monkey and a matching aESC line from a single embryo through embryo splitting. To achieve this, we conducted both symmetric and asymmetric embryo splitting (Fig. 4a). We transferred a total of twenty-two 2/4th embryos at d.p.f.6–14 female surrogates, and used the remaining matching twenty-two 2/4th embryos for ESC derivation. As a result, six surrogates became pregnant with singletons, and we obtained twelve spESC lines. Of these, one spESC line was genetically matched with a 2/4th embryo-derived newborn monkey (Supplementary Fig. 3c). In short-tandem repeat (STR) analysis, we found that 17 STR loci (originated from the parents) were identical between the 2/4th embryo-derived newborn monkey and the spESC line (Fig. 4e). These results demonstrate that a rhesus monkey (sp-monkey #1) along with its aESC line were indeed successfully established from a 2/4th embryo (Fig. 4b). Currently, the sp-monkey #1 is three years old and growing healthily under human care.

As shown above, we observed a significant difference in the number of Epi cells in genetically matched 2/4th embryos at d.p.f.8 (Fig. 1i), and an insufficient number of Epi cells in split mouse embryos (less than four) is known to hinder fetal development[32], while rhesus monkey blastocysts with a higher cell number are more likely to successfully initiate pregnancy[42]. Hence, the low efficiency in obtaining aESCs may be due to the unintended selection of 2/4th embryos with lower Epi cell counts for transfer within genetically matched pairs. Conversely, asymmetric embryo splitting allows the selection of 5/8th embryos for transfer, characterized by a profile similar to 2/4th embryos that contain a greater number of Epi cells (Fig. 1k).

Hence, we cryopreserved a total of twenty-six 5/8th embryos at d.p.f. 5–6 for transplantation and used the remaining twenty-six matched 3/8th embryos at d.p.f. 7–8 for ESC derivation, ultimately establishing 13 spESC lines. The cryopreserved 5/8th blastocysts corresponding to the 13 spESC lines were transplanted into 13 monkey surrogates (Supplementary Fig. 3c). Three surrogate monkeys were confirmed to be pregnant (Supplementary Fig. 3a–c). One rhesus (sp-monkey #2) and one cynomolgus (sp-monkey #3) monkey were successfully born (Fig. 4b). However, one cynomolgus pregnancy was aborted at 100 days of gestation. Currently, two monkeys have survived and are growing healthily under human care. Among them, sp-monkey #3 is three months old while sp-monkey #2 is six months old. As expected, the STR analyses demonstrated that the 5/8th embryo-derived newborn monkeys and the matching spESCs from 3/8th embryos are derived from the same embryos, respectively (Fig. 4f and Supplementary Fig. 3d).

The aESCs expressed key pluripotency markers (OCT4, SOX2, NANOG) (Fig. 4c and Supplementary Fig. 3a), maintained normal female monkey karyotypes after 15 or more passages (Supplementary Fig. 3e), and demonstrated differentiation into the three germ layers in vivo (Fig. 4d). Hence, through both symmetric and asymmetric embryo splitting in non-human primates, we successfully established three live monkeys and matching aESC lines.

Establishment of iPSCs and ntESCs genetically matching aESCs

In order to establish iPSCs and ntESCs with the identical genetic background as aESCs, we derived primary fibroblasts from the ear skin of sp-monkey #1 (Fig. 5A and Supplementary Fig. 3f). Subsequently, we successfully established two iPSC lines (Fig. 5B). To derive ntESCs, we followed previously established protocols for performing somatic cell nuclear transfer (SCNT)[43]. We successfully generated a total of twenty-six SCNT embryos derived from monkey fibroblasts, seven of which developed into blastocysts at d.p.f.6 (Supplementary Fig. 3g). Among these, six expanded or hatching SCNT blastocysts were used for ntESCs derivation, which gave rise to one ntESC line (Fig. 5B). The iPSCs and ntESCs expressed pluripotency genes (Fig. 5C), differentiated into three germ layers in vivo (Supplementary Fig. 3h), and maintained normal karyotypes after 15 or more passages (Supplementary Fig. 3i).

Consequently, we successfully generated genetically matched monkey iPSCs, ntESCs, and aESCs.

aESCs and ntESCs exhibit less heterogeneity in differentiation potentials compared to iPSCs

To compare the single-cell transcriptome characteristics of aESCs, iPSCs, and ntESCs with the same genetic background, we performed scRNA-seq on these PSCs cultured on feeder layers and feeder-free layers (Fig. 6a). After strict quality control, we obtained a total of 20,415 single cells from PSCs cultured on feeder layers (6788 aESCs, 5471 iPSCs, and 8156 ntESCs) and 19,727 single cells from PSCs cultured on feeder-free layers (5942 aESCs, 8735 iPSCs and 5050 ntESCs) (Supplementary Fig. 4a–c). Using uniform manifold approximation and projection (UMAP) analysis, we identified 11 and 3 cell clusters in PSCs cultured on feeder layers and feeder-free layers, respectively (Supplementary Fig. 4d, e). We confirmed that all cells were PSCs by checking that known pluripotency genes were expressed in cell clusters (Supplementary Fig. 4d, e)[40,41] and comparing them with Epi from cynomolgus monkey embryos cultured in vitro at d.p.f.10–14 using Pearson's correlation analysis (Supplementary Fig. 4f, g)[44].

https://doi.org/10.1038/s41467-025-60694-5

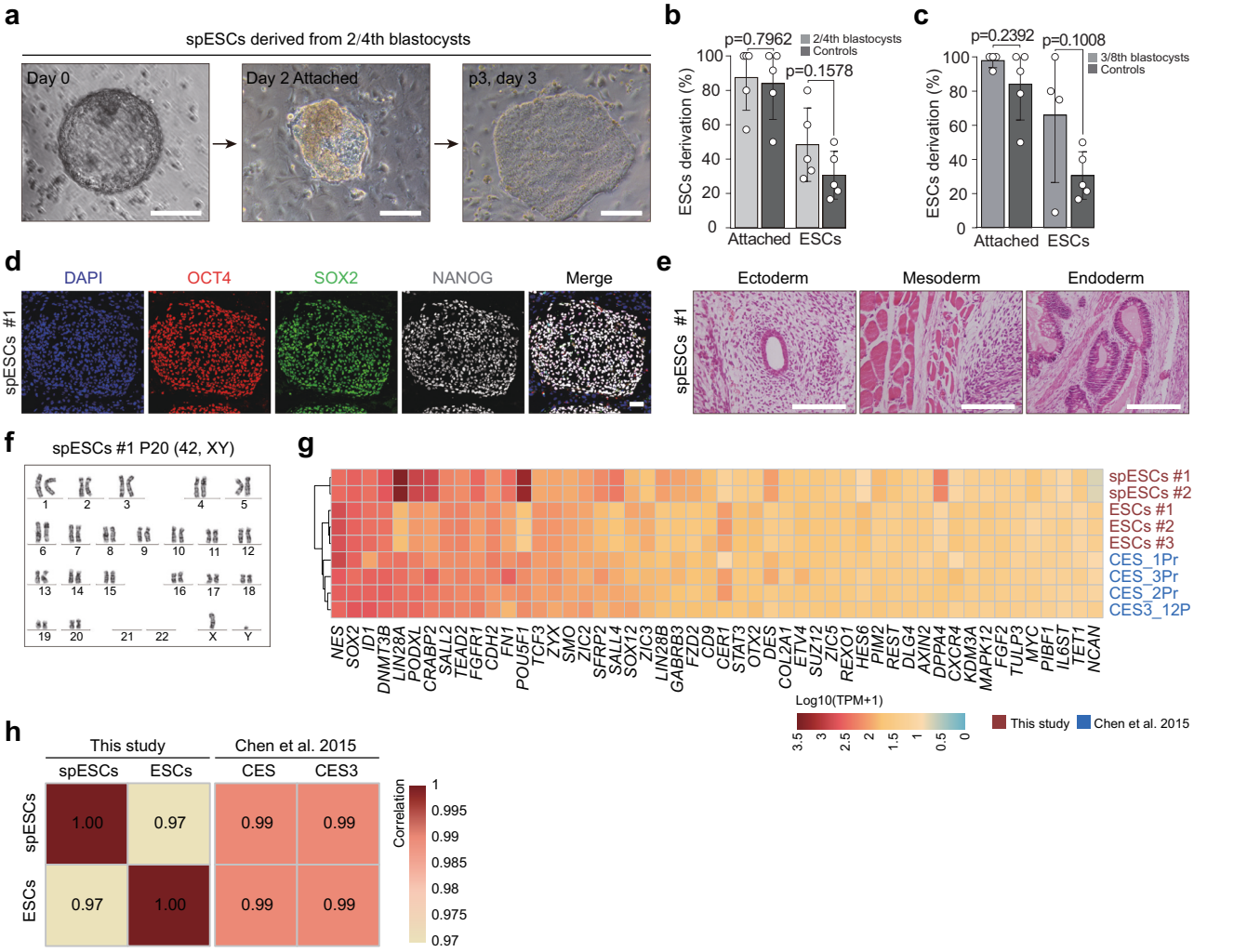

Fig. 2 | SpESC derivation from split embryos. a Representative images showing the derivation process of spESCs from 2/4th blastocyst. **b**, **c** Comparison of spESC derivation efficiency between split blastocysts and control blastocysts with statistical differences assessed using a t-test. **b** (2/4th blastocysts, n = 25, 3/8th blastocysts, n = 26; controls, n = 45), **c** (3/8th blastocysts, n = 26; controls, n = 45). Data from 4 independent experiments are shown as mean ± SEM. The statistical analysis utilized the unpaired two-tailed Student's t-test without adjustment. **d** Representative IF images of spESC were stained for pluripotency markers OCT4, SOX2, and NANOG. Similar results were obtained in no less than three independently repeated experiments. Scale bar, 100 μm. **e** Histological analysis of teratomas formed by spESCs demonstrated their ability to differentiate into the three germ layers in vivo. Similar results were obtained in no less than three independently repeated experiments. **f** Karyotype analysis of the spESCs showed a normal karyotype. **g** Heatmap showing the expression of pluripotency genes in spESCs, ESCs, and CES (previously reported primed cynomolgus monkey ESCs)[39]. The ESCs were derived from control blastocysts in our laboratory. **h** Heatmap of the correlation coefficient showing a high correlation between spESCs and ESCs based on co-expressed genes in all cells. See also Supplementary Fig. 2f. Source data are provided as a Source Data file.

We further defined the states of these cell clusters through correlation analysis between our data and a human gastrula Carnegie stage 7 (CS7) dataset[45], marker genes analysis, and lineage bias probabilities calculated by FateID (See Materials and Methods)[46]. Most cell clusters were annotated as "Epi" cells, with a few cell clusters annotated as PSCs with differentiation propensity (DPR). Taken together, we identified a total of seven distinct cell populations in the feeder layer-cultured PSCs, including Epi1, Epi2, endoderm (Endo) DPR, mesoderm (Meso) DPR, neural ectoderm (NE) DPR, non-neural ectoderm (NNE) DPR, and extraembryonic mesenchyme (ExE mech) DPR (Fig. 6b, d and Supplementary Fig. 5d). Conversely, only two cell populations were annotated in the feeder-free layer-cultured PSCs comprising Epi and ExE mech DPR (Fig. 6c, e, and Supplementary Fig. 5k).

By comparing the proportions of Epi cells and PSC with DPR, we observed that more than 80% of aESCs and ntESCs cultured on feeder layers were Epi cells without DPR. In contrast, 60% of iPSCs were Epi cells without DPR and an increased proportion of PSC showing different DPR (Fig. 6f). However, we did not observe any differences in cell type proportions among aESCs, iPSCs, and ntESCs cultured on feeder-free layers, with a negligible percentage of PSC cells with DPR (Fig. 6g). The findings suggest that both aESCs and ntESCs show reduced heterogeneity in differentiation potentials than iPSCs when cultured on a feeder layer. In contrast, the feeder-free culture conditions are more effective in reducing heterogeneity in differentiation potentials for all three types of aESCs, iPSCs, and ntESCs.

Transcriptomic signatures of aESCs, iPSCs, and ntESCs

Next, we compared the transcriptional signatures of iPSCs and ntESCs to those of aESCs using Epi cells without DPR. Compared to aESCs, we detected a greater number of differentially expressed genes (DEGs) in iPSCs than ntESCs under two culture conditions (Fig. 6h and Supplementary Data 3), suggesting a large difference between iPSCs and aESCs. Moreover, the number of DEGs in PSCs cultured under feeder-free conditions was significantly reduced relative to PSCs cultured on

https://doi.org/10.1038/s41467-025-60694-5

a

Method	Species	Blastocysts	Surrogates	Pregnancys (%)	Implanted embryos (%)	Fetuses (%)	Live births (%)	Survival infants (%)
2/4th embryo	cynomolgus	27	16	6 (37.5%)	6 (22.2%)	6 (22.2%)	5 (18.5%)	5 (18.5%)
	rhesus	10	5	2 (40.0%)	2 (20.0%)	2 (20.0%)	2 (20.0%)	2 (20.0%)
5/8th embryo	cynomolgus	4	4	2 (50.0%)	2 (50.0%)	2 (50.0%)	1 (25.0%)	1 (25.0%)
	rhesus	9	9	1 (11.1%)	1 (11.1%)	1 (11.1%)	1 (11.1%)	1 (11.1%)
Control	cynomolgus	40	25	8 (32.0%)	8 (20.0%)	8 (20.0%)	7 (17.5%)	7 (17.5%)
	rhesus	18	10	4 (40.0%)	4 (22.2%)	4 (22.2%)	4 (22.2%)	4 (22.2%)

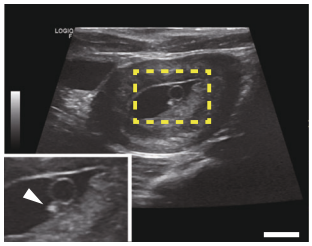

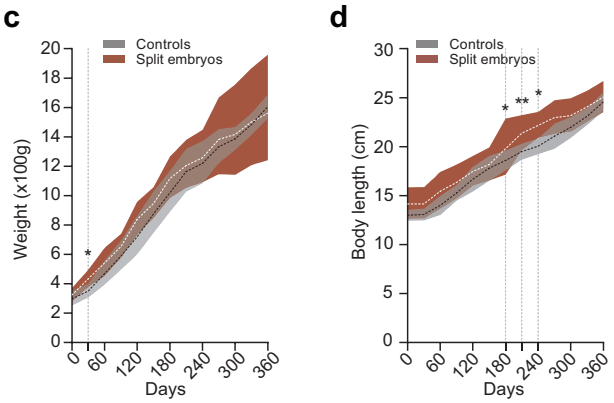

Fig. 3 | Generation of healthy monkeys from split embryos. a Post-implantation development of monkey control and split embryos. **b** An ultrasound image showing a surrogate uterus with a gestational sac containing a representative 25-day-old fetus (indicated by the yellow dashed box). The white arrowhead points to the fetus. Scale bar, 1 cm. **c**, **d** The height and weight of newborn cynomolgus monkeys derived from split embryos were continuously monitored from birth until 360 days of age. Data are displayed as mean ± SEM. White and black dashed lines indicate the mean values of split embryos and control embryos, respectively. The shaded area represents the 95% confidence interval, reflecting the variability of the data (split embryos, n = 5; controls, n = 7). The upper and lower edges of the shaded area represent the maxima and minima, respectively. The statistical analysis utilized multiple two-tailed t-tests without adjustment. *p value < 0.05, **p value < 0.01. Source data are provided as a Source Data file.

feeder layers (Fig. 6h, Supplementary Fig. 6a, b, and Supplementary Data 3). These results suggest that feeder-free culture conditions reduce the differences between iPSCs and aESCs, as well as ntESCs and aESCs. Relative to aESCs, DEGs in iPSCs in the feeder layer culture system (fold change (FC) > 1 or <1 and p-value < 0.05) were associated with maintenance of genomic stability, such as DNA duplex unwinding, DNA geometric change, DNA replication, and initiation of DNA replication (Fig. 6i). In addition, when assessing genomic instability by gene expression scoring of associated gene sets, including double-stranded break (DSB) repair, other repair pathways, replication, checkpoint, and messenger ribonucleoprotein (mRNP) biogenesis[47], we noted higher scores for replication, DSB repair, and other repair pathways in iPSCs and ntESCs cultured on feeder layers compared to aESCs. However, checkpoint and mRNP biogenesis scores were lower in iPSCs and ntESCs (Supplementary Fig. 6c). When cultured on feeder-free layers, ntESCs exhibited higher scores for DSB repair and other repair pathways compared to aESCs. In contrast, iPSCs showed no significant difference in scores for DSB repair and other repair pathways but differed significantly from aESCs in terms of scores for replication, checkpoint, and mRNP biogenesis pathways (Supplementary Fig. 6c). Beyond assessing genomic instability via gene expression scoring, we also inferred copy number variations (CNVs) using the inferCNV method. The results revealed that aESCs consistently exhibited the lowest CNV levels under both culture conditions (Fig. 6j). Collectively, these findings imply that aESCs potentially maintain genomic stability better than iPSCs and ntESCs.

Previous studies have shown that transcriptional noise in cells tends to increase with aging[48,49]. Additionally, elevated transcriptional noise is associated with exit from pluripotency[50]. To assess the transcriptional noise in aESCs, iPSCs, and ntESCs, we employed a previously reported method[48]. We found that the lowest levels of transcriptional noise under two culture conditions are consistently found in aESCs (Fig. 6k). Furthermore, when we compared the coefficients of variation of the top 100 genes contributing to transcriptional noise across the three types of PSCs, the results further support that aESCs had the lowest levels of transcriptional noise (Supplementary Fig. 6d). Notably, the ntESCs showed a similar pattern to the iPSCs (Fig. 6j and Supplementary Fig. 6d). Functional enrichment analysis suggests the conserved function and importance of these genes (Supplementary Fig. 6e). In summary, the results may suggest that aESCs exhibited the lowest levels of transcriptional noise under two culture conditions.

In conclusion, our findings reveal a closer transcriptional similarity between ntESCs and aESCs compared to iPSCs. Notably, feeder-free culture conditions further diminish these transcriptional discrepancies. Furthermore, aESCs may maintain genomic stability more effectively and exhibit lower transcriptional noise compared to iPSCs and ntESCs, but further investigation is needed to confirm these potential differences.

Derivation of human ESCs from split embryos

Given our successful generation of monkey aESCs, we investigated the feasibility of deriving human ESCs (hESCs) from human split embryos. Thus, we thawed a total of nine 8- to 16-cell human embryos at d.p.f.3 and separated these into 18 split embryos by symmetric embryo splitting, 13 of which developed into blastocysts at d.p.f.5 (Supplementary Fig. 7a, g). The developmental process in split embryos, involving compaction and morula formation at d.p.f.4, followed by blastocyst formation at d.p.f.5, was consistent with that observed in control embryos (Fig. 7a)[51]. Subsequently, when we performed IF analysis to determine the number of ICM cells and total cells in split embryos at d.p.f.6 (Fig. 7b), we documented significant differences compared to control embryos (Fig. 7c and Supplementary Fig. 7f). However, there were no significant differences in the proportion of

https://doi.org/10.1038/s41467-025-60694-5

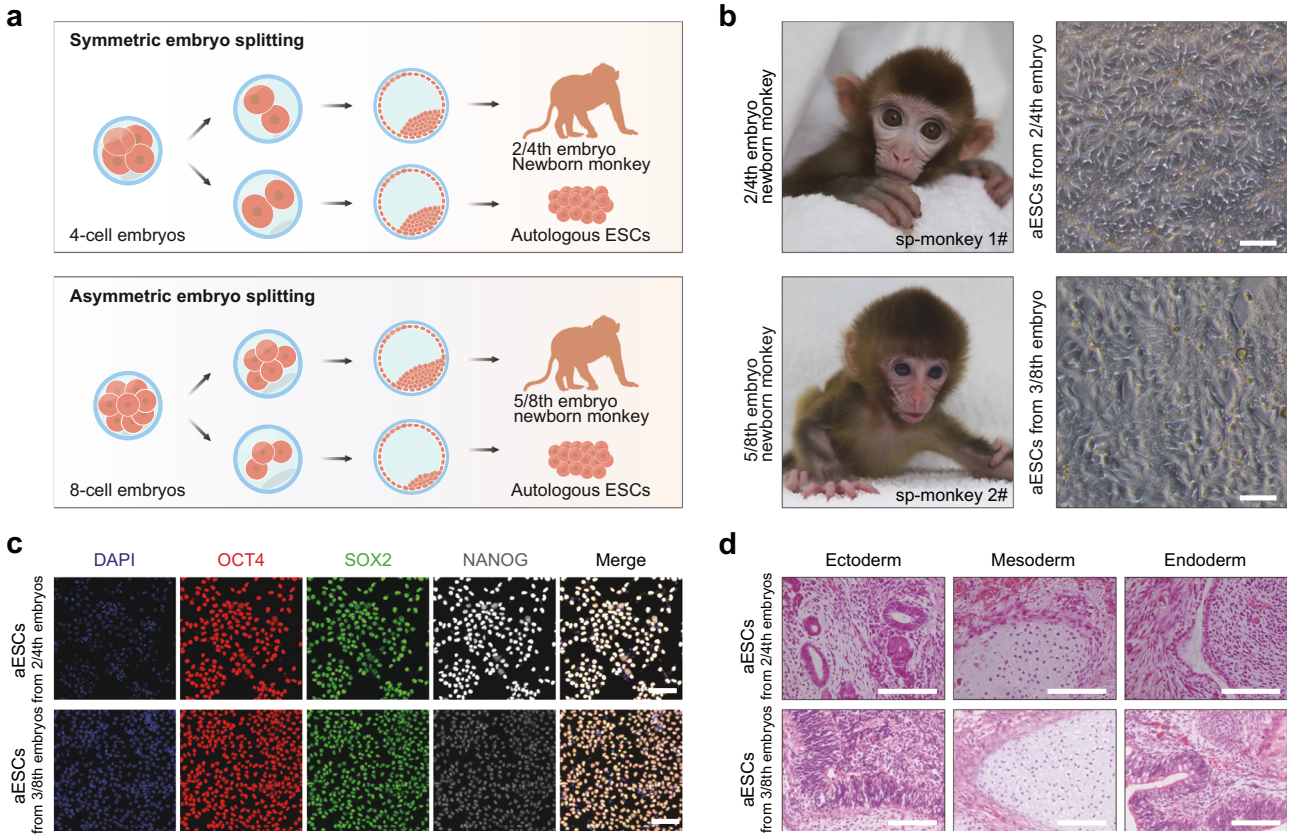

e

STR loci	aESCs from 2/4th embryo	sp-monkey 1#	Oocyte donor	Sperm donor	Surrogate
D2S102	145/154	145/154	154/167	145/157	156/165
D5S820	191/199	191/199	191/199	187/191	176/183/187
D6S2741	177/203	177/203	177/196	177/203	177/199
D6S311	243/245	243/245	233/235/245	236/243	220/233
D7S1827	132/140	132/140	132/140	132/150	132/140
D8S1106	135/140	135/140	135/156	140/144	140
D10S1432	162/166	162/166	162/166	157/162	157/162
D12S86	127/129	127/129	113/129	127	118/127/129
D13S765	228	228	228/254	216/228	216/224
D14S3306	175/182	175/182	171/175	178/182	175/183
D15S644	195/236	195/236	225/236	195/261	232/236
D16S415	185/197/216	185/197/216	182/197/222	185/197/216	180/198/210
D17S1290	172/176	172/176	172/176	176/229	172/176
D18S536	150/160	150/160	160	150/155/160	149/160
D19S255	113/120/141	113/120/141	120/140	113/141	129/141
D21S1256	221/281	221/281	221	220/281	221/281
DXS8043	188/190/202	188/190/202	201/202	178/188/190	202/204/206

f

STR loci	aESCs from 3/8th embryo	sp-monkey 2#	Oocyte donor	Sperm donor	Surrogate
D2S102	147/154	147/154	147/166	147/154	131/170
D5S820	182/198	182/198	182/215	186/198	190/194
D6S2741	195/203	195/203	195/201	203/215	209/211
D6S311	236/246	236/246	218/246	230/236	236/240
D7S1827	131/145	131/145	131	140/145	126/131
D8S1106	135/144	135/144	135	144/176	153
D10S1432	144/153	144/153	153/165	144/161	157/161
D12S86	121/125	121/125	121	125/128	110/125
D13S765	221/226	221/226	217/221	213/226	217/234
D14S3306	166/173	166/173	173/181	166/173	170/188
D15S644	226	226	217/226	221/226	218/238
D16S415	196/204	196/204	194/204	191/196	211/219
D17S1290	238/242	238/242	234/238	242	226/250
D18S536	160	160	156/160	160	156/160
D19S255	112/116	112/116	112/116	112	112/116
D21S1256	221	221	221	221	221
DXS8043	190/200	190/200	200/208	190	182/202

Fig. 4 | Generation of aESCs and monkey from single embryos. a Schematic diagram illustrating the experimental procedures. **b** Images of 2/4th and 3/8th embryos giving rise to newborn monkeys at 150 and 20 days after birth, respectively. Representative bright-field images of aESCs derived from 2/4th embryos and 3/8th embryos. Similar results were obtained in no less than three independently repeated experiments. **c** Representative IF images of aESCs from 2/4th and 3/8th embryos were stained for pluripotency markers OCT4, SOX2, and NANOG. Similar results were obtained in no less than three independently repeated experiments. **d** Histological analyses of teratomas formed by the aESCs revealed their potential to differentiate into all three germ layers in vivo. Similar results were obtained in no less than three independently repeated experiments. **e**, **f** Genetic analysis based on STRs examination shows that the nuclear DNA of the three-year-old and six-month-old monkey is consistent with that of aESCs but different from that of surrogate monkeys. The nuclear DNA of the newborn monkey and aESCs originated from their parents. All scale bar, 100 μm.

OCT4 and NANOG-positive cells relative to total cells between split embryos and control embryos at d.p.f.6 (Fig. 7d, e). These results indicate that the split embryos were able to develop into blastocysts and form ICM with only a proportional reduction in the number of cells.

To derive ESCs from split embryos, we cultured a total of four pairs of eight split embryos at d.p.f.6 on mouse embryonic fibroblast (MEF) feeders (Supplementary Fig. 7b). On the second day, all split embryos had successfully attached, and we observed outgrowth in three split embryos derived from distinct embryos, resulting in the establishment of three hESC lines (Fig. 7f and Supplementary Fig. 7c). These hESC lines expressed key pluripotency marker genes, including OCT4, SOX2, and NANOG (Fig. 7g and Supplementary Fig. 7d), and maintained normal karyotypes after 15 or more passages (Supplementary Fig. 7e). Additionally, bulk RNA-seq analysis revealed the expression of 50 known pluripotency genes at levels comparable to published human ESCs (Fig. 7h)[28–31,40,41]. Moreover, in correlation analysis of gene expression patterns, we found a robust correlation between the three hESCs and previously published hESCs[28–31], indicating a high degree of similarity in gene expression profiles (Fig. 7i).

In conclusion, we successfully derived and characterized hESCs from human split embryos, providing evidence for the feasibility of establishing autologous hESCs through embryo splitting.

https://doi.org/10.1038/s41467-025-60694-5

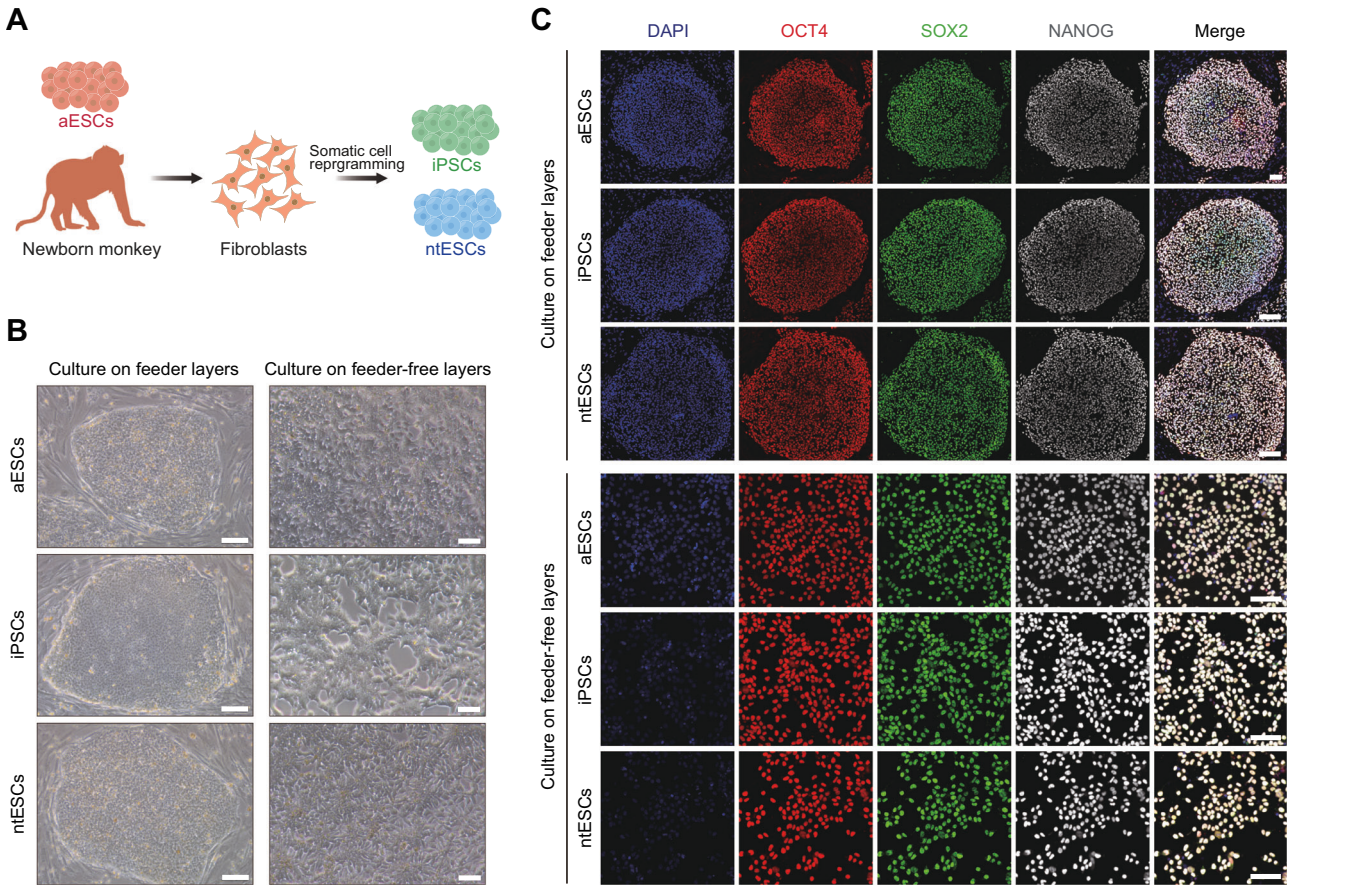

Fig. 5 | Characterization of genetically matched aESCs, iPSCs, and ntESCs cultured on feeder and feeder-free layers. A Schematic diagram of the experiment. **B** Bright-field showing typical cell morphology of genetically matched aESCs, iPSCs, and ntESCs cultured on feeder and feeder-free layers. Similar results were obtained in no less than three independently repeated experiments. **C** Representative IF images of genetically matched aESCs, iPSCs, and ntESCs cultured on feeder and feeder-free layers and stained for pluripotency markers OCT4, SOX2, and NANOG. Similar results were obtained in no less than three independently repeated experiments. All scale bar, 100 μm.

Discussion

In this study, we successfully generated monkey aESCs and demonstrated the potential application of embryo splitting technology to human embryos. The aESCs had the same genetic background as the individual monkeys from the same embryonic origin and exhibited highly similar developmental characteristics to ESCs derived from normal embryos. Previous studies comparing ESCs and iPSCs have been challenged by genetic background variability[52–57]. Here we report the derivation of three PSCs with consistent genetic backgrounds and conduct a comparative analysis of their transcriptomic characteristics at the single-cell level under different culture conditions. Our approach enables a comprehensive comparison among the three types of PSCs in primates, eliminating genetic background and culture condition influences.

We observed that iPSCs, compared to aESCs and ntESCs, exhibited a higher degree of heterogeneity and a tendency for differentiation, indicative of abnormal epigenomics[7,8,58,59]. This phenomenon is notably conspicuous in the feeder culture condition, which sustains the cells in a primed state[39,60]. In our detailed comparison of the epiblast cell population, we found that iPSCs exhibited more substantial differences in transcriptomic characteristics compared to aESCs under both culture conditions. The majority of DEGs were associated with critical processes such as DNA replication, genomic stability, and cell cycle regulation. Within iPSCs, genes like *NNAT*, *IGFBP2*, *SLC2A1*, and *BNIP3* showed significant differences in both culture conditions compared to aESCs. Previous studies have suggested these genes are directly associated with the maintenance and rejuvenation of pluripotency in stem cells[61–64]. However, further research is necessary to elucidate the functional differences among these three types of PSCs. In addition to differential expression analysis, CNV analysis revealed that aESCs consistently exhibited the lowest CNV levels across both culture conditions. Overall, aESCs maintain better genomic stability compared to iPSCs and ntESCs. Furthermore, transcriptome noise analysis within the epiblast cell group among the three PSC types revealed that aESCs possessed the lowest levels of transcriptome noise. ESCs offer a number of advantages, including differentiation efficiency, genetic stability, epigenetic memory, and reproducibility. Our study data confirm that aESCs (spESCs) closely resemble ESCs derived from normal blastocysts. However, aESCs are currently unable to fully replace the significant advantages of iPSCs. Furthermore, the future clinical application of aESCs as autologous stem cell replacement requires additional support through further differentiation and in vivo studies, including safety assessments, immune rejection evaluations and efficacy investigations.

In this study, we used 4-cell and 8-cell monkey embryos for embryo splitting experiments. Although both methods yielded blastocyst development rates consistent with normal embryos, we observed a discrepancy in the numbers of Epi cells in the 2/4th blastocysts derived from the same embryo, with one having fewer Epi cells. This discrepancy might explain the reduced efficiency in obtaining aESCs using this method (1/22, 4.5%), underscoring that Epi cell count is a crucial determinant for successful implantation[32,42]. When implementing the 3:5 ratio splitting method at the 8-cell stage, we again observed a disparity in Epi numbers between two split blastocysts. Consequently, we prioritized blastocysts with a higher Epi count for

https://doi.org/10.1038/s41467-025-60694-5

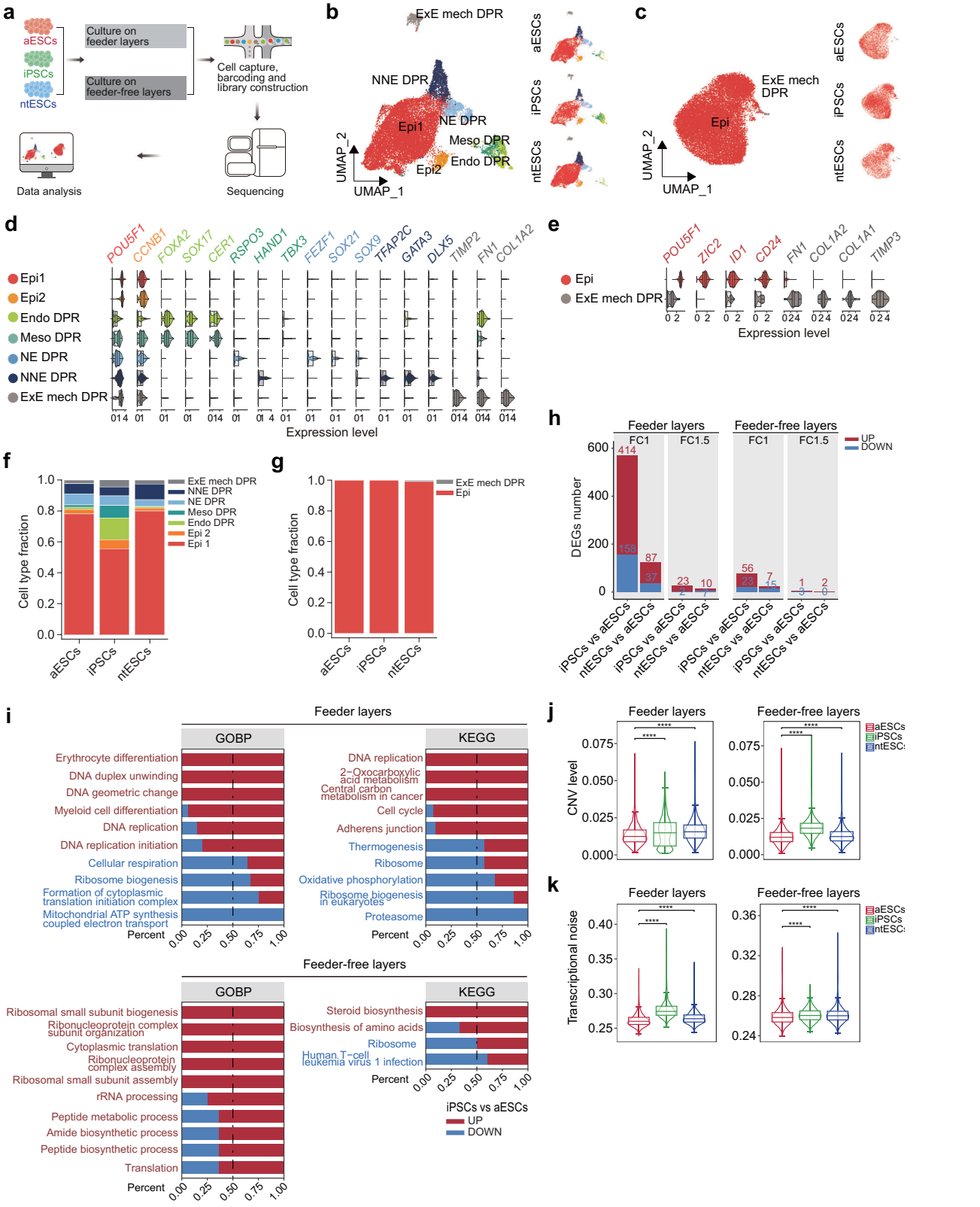

embryo transfer and used those with a lower Epi count for establishing ESCs. This strategic approach increased the efficiency of obtaining aESCs (3/26, 11.5%). Such heterogeneity in the early embryo may help explain inconsistent Epi numbers observed in 2/4th blastocysts[32–36,65,66], but further investigation is warranted to validate stronger conclusions in monkeys. Moreover, deriving ESCs from split embryos with fewer blastomeres or from individual blastomeres[23–25], and transplanting split embryos matched to these ESCs, may potentially further enhance the differentiation efficiency of aESCs. However, the comparability between ESCs derived from single blastomeres and those from normal blastocysts requires thorough evaluation, as the former have not undergone blastocyst formation.

In conclusion, our study not only presents an innovative approach to generate autologous pluripotent stem cells from split embryos but

Fig. 6 | Maintenance of stem cell characteristics and genomic stability across aESCs, iPSCs, and ntESCs. a Schematic diagram of experiment. **b** UMAP visualization showing seven different cell types in PSCs cultured on a feeder layer, each represented by a distinct color. Each stem cell type is shown separately on the right. **c** UMAP visualization showing two cell types in PSCs feeder-free PSC, cultured on the feeder-free layer, each represented by a distinct color. Each stem cell type is shown separately on the right. **d**, **e** Violin plots depicting expression levels of key lineage-associated genes across seven cell types in the feeder layer and two cell types in the feeder-free layer, respectively. Endo differentiation propensity (DPR) expressed genes associated with endoderm development, including *FOXA2*, *SOX17*, and *CER1*[44,45]. Meso DPR exhibited elevated expression of genes related to mesoderm formation, such as *RSPO3*, *HAND1*, and *TBX3*[44,45]. NE DPR expressed early neural cell lineage markers *FEZF1*[77,78] and genes promoting stem cell differentiation into neural cells, such as *SOX21* and *SOX9*[79–82]. NNE DPR upregulated non-neuroectoderm genes *TFAP2C*, *GATA3*, *DLX5*, and *CLDN10*[45]. ExE mech DPR upregulated ExE mech genes *TIMP1*, *FN1*, and *COL1A2*[37,83,84]. **d** seven cell types are represented: Epi1 (n = 14864 cells), Epi2 (n = 650 cells), Endo DPR (n = 949 cells), Meso DPR (n = 567 cells), NE DPR (n = 1162 cells), NNE DPR (n = 1607 cells), and ExE mech DPR (n = 616 cells). These data are from one biological replicate of iPSCs, aESCs, and ntESCs. **e** two cell types are shown: Epi (n = 19669 cells) and ExE mech DPR (n = 57 cells), derived from one biological replicate of iPSCs, aESCs, and ntESCs. For the box plots, the central line represents the median, the box boundaries correspond to the 25th and 75th percentiles. The length of the whiskers indicates 1.5 times the interquartile range from the first and third quartiles. **f**, **g** Comparison of heterogeneity in constituent cell types among aESCs, iPSCs, and ntESCs cultured on feeder layers and feeder-free layers, respectively. **h** The number of up- and down-regulated DEGs with FC > 1 or <1 and p-value < 0.05, as well as FC ≥ 1.5 or ≤ 0.67 and p-value < 0.05, in iPSCs and ntESCs cultured with and without feeder layers, compared to aESCs. Red and blue values on the bars represent the number of up- and down-regulated DEGs. Gene expression differences were compared using two-sided Wilcoxon Rank-Sum test. Due to the small number of DEGs, p values were not adjusted using the Benjamini-Hochberg method. **i** The top 10 Gene Ontology (GO) terms and KEGG pathways were identified through functional enrichment analysis, based on DEGs (FC > 1 or <1 and p-value < 0.05). For GO terms, p-values were adjusted using the Benjamini-Hochberg method. For KEGG pathways, due to the small number of DEGs, p-values were not adjusted using the Benjamini-Hochberg method. **j**, **k** Violin plots showing the differences in CNV level and transcriptional noise in Epi cells derived from the three PSC types (aESCs, iPSCs, and ntESCs). For feeder layer, n = 5301 cells from one biological replicate of aESCs, n = 3038 cells from one biological replicate of iPSCs, n = 6525 cells from one biological replicate of ntESCs. For feeder-free, n = 5929 cells from one biological replicate of aESCs, n = 8733 cells from one biological replicate of iPSCs, n = 5007cells from one biological replicate of ntESCs. The differences in CNV level and transcriptional noise were compared by two-sided Wilcoxon Rank-Sum test, with p < 0.0001 indicated by ****. For the box plots, the central line represents the median, the box boundaries correspond to the 25th and 75th percentiles. The length of the whiskers indicates 1.5 times the interquartile range from the first and third quartiles.

also offers valuable insights into the characteristics of aESCs compared to iPSCs and ntESCs. These findings highlight the potential of aESCs in developing stem cell therapies, paving the way for further investigation into their therapeutic applications. However, limitations such as applicability to IVF offspring, cost-effectiveness, and safety risks of transferring split versus intact embryos must be addressed. Notably, we propose an approach of completely separating and reassembling blastomeres into two split embryos. This method may offer potential advantages in rearranging spatial structure and ensuring proper gene expression, enabling the split embryos to follow a normal developmental clock to reach the blastocyst stage successfully. Consequently, hESCs can be derived from human split embryos at d.p.f.6 successfully. This successful derivation suggests that it might be feasible in the future to obtain human aESCs through assisted reproductive technologies and cryopreserve these for possible future therapeutic use, with careful consideration of ethical concerns.

This study has limitations that should be acknowledged. First, despite advancements in asymmetric embryo splitting, the derivation of monkey aESCs remains challenging, with room for increased efficiency. This optimization may broaden the applicability of our findings. Second, the scRNA-seq analysis was conducted with a limited number of cell lines. Although it provides valuable insight into the transcriptomic signatures of three cell types, individual differences may affect the results. Therefore, future studies should prioritize additional biological replicates to strengthen the robustness of conclusions. Third, the preliminary data from the study does not fully support our hypothesis on the comparative advantages of aESCs over ntESCs and iPSCs in terms of genetic stability and transcriptional noise. This highlights the need for future research to explore these aspects more comprehensively, which could lead to a clearer understanding of the distinct benefits associated with each cell type. Lastly, while live births and trophectoderm (TE) marker expression confirm partial functionality of split embryo-derived TE cells, their capacity to form functional trophoblast stem cells (TSCs) and support full placental development requires validation through TSCs isolation experiments.

Methods

Ethics statement

In this study, the use of human embryos was approved by the Medicine Ethics Committee of The First People's Hospital of Yunnan Province (KHLL2020-KY064). The process of obtaining informed consent for embryo donation followed the 2016/2021 guidelines set by the International Society for Stem Cell Research (ISSCR) and the 2003 Ethical Guidelines for Human Embryonic Stem Cell Research jointly issued by China's Ministry of Science and Technology and Ministry of Health. All donating couples voluntarily signed consent forms to donate their surplus embryos for research purposes. No financial inducements were provided for the donations.

The ethical treatment of primates during all procedures involving non-human primates was conducted following the guidelines established by the Association for Assessment and Accreditation of Laboratory Animal Care International (AAALAC). The ethics application was approved by the State Key Laboratory of Primate Biomedical Research (LPBR202001018).

Monkeys

Healthy rhesus monkeys *(Macaca mulatta)* and cynomolgus monkeys *(Macaca fascicularis)*, ranging in age from 5–12 years with body weights of 4–8 kg, were selected for use in this study. All animals were housed at the State Key Laboratory of Primate Biomedical Research.

Semen collection

Healthy male cynomolgus and rhesus monkeys were anesthetized with an intramuscular injection of ketamine hydrochloride (4 mg/kg). Their penises and scrotums were washed with saline. Two aluminum foil strip electrodes, wrapped in defatted cotton and soaked in saline, were placed at both ends of the penis. Semen was collected using a semen collector (Grass, S44) through intermittent stimulation. After 30 minutes of liquefaction at 37 °C, the semen was centrifuged at 150 × g for 3 minutes to remove the seminal plasma. The resulting samples were stored at room temperature for future use.

Oocyte collection, ICSI, embryo culture, and embryo transplantation

In brief, 20 healthy female rhesus monkeys and 20 healthy female cynomolgus monkeys aged 5–12 years with regular menstrual cycles were selected as oocyte donors for superovulation, which was performed by intramuscular injection with rhFSH (Merck Serono, recombinant human follitropin alpha, GONAL-F) for 8 days, then rhCG (Merck Serono, recombinant human chorionic gonadotropin alpha, OVIDREL) was injected on day 9. Oocytes were collected by laparoscopic follicular aspiration 32–35 hours after rhCG administration.

https://doi.org/10.1038/s41467-025-60694-5

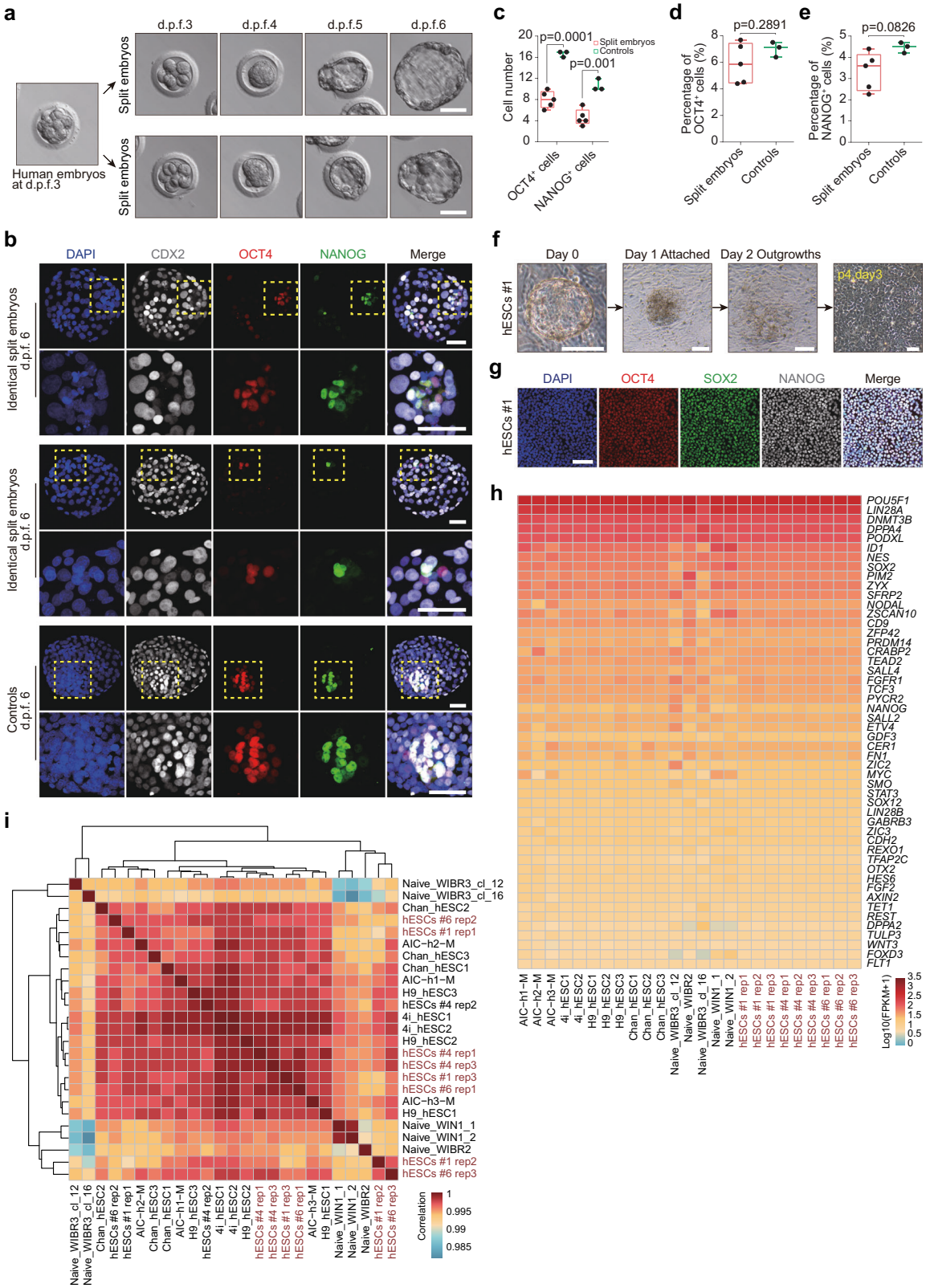

Follicular contents were placed in Hepes-buffered Tyrode's albumin lactate pyruvate (TALP) medium containing 0.3% BSA at 37 °C. Oocytes were stripped of cumulus cells by pipetting after a brief exposure (<1 min) to hyaluronidase (0.5 mg/ml) in TALP-Hepes to allow visual selection of nuclear maturity metaphase II (MII; first polar body present) oocytes. The mature oocytes were subjected to intracytoplasmic sperm injection (ICSI) immediately and then cultured in CMRL-1066 (Gibco, 11530037) containing 10% fetal bovine serum (FBS) at 37 °C in 5% CO2. Fertilization was confirmed by the presence of the second polar body and two pronuclei. Zygotes were then cultured in the chemically defined hamster embryo culture medium-9 (HECM-9) containing 10% fetal bovine serum at 37 °C in 5% CO_2 to allow embryo development. The culture medium was replaced every other day until the blastocyst stage. The embryos were cultured up to d.p.f.10 using

Fig. 7 | Characterization of hESCs derived from split embryos. a Representative bright-field developmental progression of human split embryos in vitro. Similar results were obtained in no less than three independently repeated experiments. Scale bar, 100 μm. **b** Representative IF images of identical split embryos at d.p.f.6 stained for CDX2, OCT4, NANOG, and DAPI (split embryos, n = 5; controls, n = 3). Scale bar, 50 μm (long) and 100 μm (short). **c** The number of ICM cells compared across split embryos and controls at d.p.f.6, with each dot representing one blastocyst (split embryos, n = 5; controls, n = 3). Data from 3 independent experiments are shown as mean ± SEM. The upper and lower edges of the box represent the maxima and minima, respectively, while the thick lines in the middle indicate the mean of each sample. The statistical analysis utilized the unpaired two-tailed Student's t-test without adjustment. **d**, **e** The percentage of $OCT4^+$ and $NANOG^+$ cells out of the total number of cells (DAPI) (split embryos, n = 5; controls, n = 3). Data from 3 independent experiments are shown as mean ± SEM. The upper and lower edges of the box represent the maxima and minima, respectively, while the thick lines in the middle indicate the mean of each sample. The statistical analysis utilized the unpaired two-tailed Student's t-test without adjustment. **f** Representative images showing the derivation process of hESCs from split blastocyst. Similar results were obtained in no less than three independently repeated experiments. **g** Representative IF images of hESCs were stained for pluripotency markers OCT4, SOX2, and NANOG. Similar results were obtained in no less than three independently repeated experiments. Scale bar, 100 μm. **h** Heatmap showing the expression of pluripotency genes in hESCs and other human PSCs from previous works. The following datasets were used: human conventional ESCs (H9_hESC1, H9_hESC1, H9_hESC3, Chan_hESC1, Chan_hESC2, and Chan_hESC3)[28], human naïve ESCs (WIBR2, WIBR3_cl_12, WIBR3_cl_16, WIN1_1 and WIN1_2)[29], human other PSCs (AIC-h1-M, AIC-h1-M, 4i_hESC1, and 4i_hESC2)[30,31]. Brown-marked cells were generated in our lab. **i** Heatmap of the correlation coefficient showing a high correlation between hESCs derived from split embryos and other hPSCs mentioned above, based on co-expressed genes in all cells. Brown-marked cells were generated in our lab. Source data are provided as a Source Data file.

the methods described in previously published articles[37,67]. For embryo transplantation, the female monkeys, aged 5–10 years, chosen as surrogate recipients had appropriate levels of estradiol and progesterone. Each recipient received one or two embryos and ultrasound was used around day 25 after transfer to confirm pregnancy and determine the number of fetuses by detecting fetal cardiac activity and yolk sac presence.

Human embryos acquisition and culture

Human embryos used in this research were excess cryopreserved embryos from couples who had previously undergone successful in vitro fertilization therapy and conceived a healthy child. Donating these embryos did not affect their subsequent in vitro fertilization cycles. Human embryos at d.p.f.3 were thawed following the instructions provided in the thawing media kit (Kitazato Corporation, VT102) and then cultured in equilibrated G-2 culture medium (Vitrolife, 10132). The culture medium was replaced every other day until the blastocyst stage.

Construction of monkey split embryos

The 4-cell embryos were divided using symmetric embryo splitting, while the 8-cell embryos were divided using asymmetric embryo splitting in a ratio of 3:5. Specifically, the empty zona pellucida (ZP) obtained from discarded germinal vesicle (GV) oocytes were cultured in HECM-9 supplemented with 10% FBS at 37 °C and 5% CO2 until further use. To separate blastomeres, 4- or 8-cell embryos were briefly exposed (<40 seconds) to BSA-free TH3 medium containing 5 mg/ml protease (Sigma, P8811) to remove ZP. Immediately, the embryos were washed six times in TH3 medium until the ZP disappeared completely. The embryos were then transferred to Ca^{2+}/Mg^{2+}-free and BSA-free TH3 with 0.025% Trypsin-EDTA (Thermo Fisher Scientific, 15400-054) at 37 °C for five minutes to facilitate blastomere separation before being washed six more times in TH3 medium to clean any residue. The ZP-free embryos were exposed to TH3 with 5 μg/ml of cytochalasin B (Sigma, C6762) for 5 minutes and then repeatedly aspirated and blown into a 100 μm inside diameter pipette until the blastomeres separated. The blastomeres and empty ZP were transferred to a manipulation droplet of TH3 with 5 μg/ml of cytochalasin B (Sigma, C6762) on the center of dishes covered with 3 ml mineral oil (Sigma, 8042-47-5). The blastomeres were aspirated into a 50 μm injection pipette with a 30-degree oblique mouth, and then an empty ZP was held with a holding pipette. Meanwhile, the ZP was ablated using a single laser pulse, and the injection pipette containing blastomeres was immediately inserted into the hole. Next, the blastomeres were placed inside the empty ZP. The assembled embryos were washed 6 times in HECM-9 medium and then transferred to a 3.5 cm micro well group culture dish (Vitrolife, 16606) containing 16 microwells with HECM-9 medium. The embryos were cultured until they reached the blastocyst stage for ESC derivation and embryo transfer.

Construction of human split embryos

Frozen-thawed human embryos should be cultured in the medium for a minimum of one hour before they are ready for embryo splitting. Subsequently, the embryos were briefly exposed (<40 seconds) to Tyrode's solution to remove ZP. They were then transferred into Ca^{2+}/Mg^{2+}-free PBS with 0.025% Trypsin-EDTA (Thermo Fisher Scientific, 15400-054) at 37 °C for 40 seconds to facilitate blastomere separation before being washed six more times in G-MOPS medium (Vitrolife, 10130) to clean any residue. The embryos were repeatedly aspirated and blown into a pipette with an inside diameter of 100 μm to separate the blastomeres. Following the same procedure as employed for monkey embryo splitting, the isolated blastomeres were transferred into empty human ZP and cultured in G-2 medium until reaching the blastocyst stage.

Derivation and culture of spESCs and ESCs

The control blastocysts at d.p.f.7 were transiently treated with 0.5% protease to remove the ZP, and the 2/4th blastocysts at d.p.f.7–8 were hatched from the ZP. They were then cultured on feeders in feeder-cultured PSCs medium supplemented with 10 μM Y27632 (Selleck, S1049)[30]. Fresh feeder-cultured PSCs medium containing 5 μM Y27632 was added when the blastocysts attached to the feeder layer, and it was subsequently replaced every two days until ESC-like outgrowth became visible. Typically, ESC-like outgrowth appears within 7–14 days. After a brief treatment with Collagenase type IV (1 mg/ml) for approximately 10 minutes, the outgrowth is manually picked, dissociated into small clusters, and placed on a new feeder layer in PSCs supplemented with Y27632 (5 μM). Within 3–5 days, the outgrowth exhibits characteristic conventional ESC colony morphology and can be further passaged and expanded. The feeder-cultured PSCs medium was composed of DMEM/F12 (Thermo Fisher Scientific, 10565018), 15% knockout serum replacement (KSR, Thermo Fisher Scientific, A3181502), 1% nonessential amino acids (Thermo Fisher Scientific, 11140050), 0.1 mM β-mercaptoethanol (Sigma, M7522), and supplemented with 5 ng/ml bFGF (Millipore, GF003AF). Subsequently, it was mixed with hPSC XF (BI, 05-100-1 A) at a ratio of 1:4.

The 3/8th blastocysts at d.p.f.7–8 were hatched from the ZP and then seeded on feeders in feeder-free-cultured PSCs medium[38]. After 48 hours, the whole attached blastocysts were incubated with accutase for 10–15 minutes at 37 °C. All dissociated single cells were scattered onto feeders. After 3–5 days, obvious ESC colonies can be observed. Then, the colonies were dissociated into single cells using Accutase and passaged onto culture dishes coated with 50 μg/ml vitronectin. The feeder-free-cultured PSCs medium was changed daily, and the newly established ESC lines were passaged every 3–4 days at a split ratio of 1:4 to 1:10. Y-27632 or Clone R (STEMCELL, 5888) is necessary for the initial passaging and culturing. Feeder-free-cultured PSCs medium was composed of Essential 8 (Gibco, A2656101), 1 ×

Chemically Defined Lipid Concentrate (Gibco, 11905031), 1 × Glutamax (Gibco, 35050061), 1.94 mg/l L-Glutathione reduced (Sigma, G4251), 100 μg/l of Nodal (Bio-Techne, 3218-ND-025), 2 μM IWR-1 (Selleck, S7086) and 10 ng/ml of activin A (Peprotech, 120-14E). Prepared feeder-free medium could be kept at 4 °C for up to 1 week.

Derivation and culture of aESCs from monkey split blastocysts

For symmetric embryo splitting, one of the two 2/4th blastocysts derived from the same embryo was used to establish ESCs using the spESCs derivation method. Meanwhile, the matched 2/4th blastocyst was utilized for embryo transfer to obtain animals. For asymmetric embryo splitting, genetically matched 3/8th and 5/8th blastocysts were used. The 3/8th blastocyst was employed for establishing ESCs using the spESCs derivation method, while the 5/8th blastocyst was cryopreserved following the instructions provided by reagent kit (Kitazato Corporation, VT101). Once ESCs were successfully derived from the 3/8th blastocyst, the thawing process of the cryopreserved 5/8th blastocyst was carried out according to the instructions provided by reagent kit (Kitazato Corporation, VT102), followed by its subsequent transfer to obtain animals.

Primary monkey fibroblast isolation and culture

In brief, the two-month-old rhesus monkey ear skin samples were sterilized with 75% ethyl alcohol, washed with PBS, and then cut into pieces. After removing the hair and fat tissues, the pieces were adhered to the culture dish. Fibroblasts were cultured in DMEM supplemented with 10% FBS and 1% penicillin/streptomycin.

Monkey SCNT

The procedure of SCNT was carried out following previously established protocols[43]. Briefly, the MII oocytes were treated with TH3 containing 5 μg/ml cytochalasin B at 37 °C for 5 minutes, followed by the removal of the spindle using the spindle viewer system. After a brief incubation of donor fibroblasts with Sendai virus (GenomONE, ISK-CF-001-EX), the donor cells were inserted into the perivitelline space of the enucleated oocytes using a laser perforation system. The fusion was completed after 1.5 to 2 hours. For chemical activation, the reconstructed oocytes were treated with HECM-9 containing 5 μM calcium ionophore for 5 minutes, followed by incubation in HECM-9 containing 2 mM 6-dimethylaminopurine (Sigma-Aldrich, D2629) and 10 nM trichostatin A (Sigma-Aldrich, T8552) for 5 hours. After being activated for 6 hours, the mRNA of H3K9me3 demethylase KDM4D (1000 ng/μl, 10 pl) was injected. The SCNT embryos were cultured to the blastocyst stage and utilized for establishing ESC lines.

Generation and culture of iPSCs and ntESCs from primary fibroblasts

The iPSC lines were generated using the Sendai Reprogramming Kit (Thermo Fisher Scientific, A16518) according to the manufacturer's instructions. Subsequently, the iPSCs were cultured using established feeder layers culture system as previously described[30]. The SCNT blastocysts at d.p.f.7 were transiently treated with 0.5% protease to remove the ZP, and cultured on feeders in feeder-cultured PSCs medium supplemented with 10 μM Y27632 (Selleck, S1049). Following the same procedure as ESCs derivation from 2/4th blastocysts, the ntESCs were cultured using established feeder layers culture system as previously described[30].

Conversion of feeder-cultured PSCs into feeder-free-cultured PSCs

The feeder layer medium was removed and washed twice with feeder-free-cultured PSCs medium. Monkey PSCs were dissociated using Accutase (Gibco, A1110501) and seeded onto Vitronectin XF (STEMCELL, 07180)-coated plates in an appropriate volume based on cell lines and growth ratio. For the first three passages, passaging was performed at high density (1:1, 2 ratio) to increase viability and proliferation rate. After 5–10 passages, stable growth of PSCs in feeder-free-cultured PSCs medium was achieved.

Derivation and culture of hESCs from human split blastocysts

The procedure for culturing feeder-dependent hESCs was conducted according to previously described methods[68]. Briefly, the human blastocysts were hatched from the ZP at d.p.f.6 and then seeded onto a feeder layer in XF hEPS medium. After 48 hours, the entire attached blastocysts were incubated with Accutase at 37 °C for 10–15 minutes to dissociate into single cells. These dissociated cells were then scattered onto a culture dish coated with Laminin 521 (Thermo Fisher Scientific, A29248). The medium was refreshed every 2 days.

Embryo immunofluorescent staining

Embryos were fixed with 4% paraformaldehyde and 0.1% polyvinyl pyrrolidone (PVP) for 15 minutes at room temperature and washed three times with PBS, and then incubated overnight with 0.3% Triton X-100 and 0.1% PVP at 4 °C. After washing with PBS three times, embryos were blocked for 2 hours in block buffer (3% bovine serum albumin + 10% fetal bovine serum + 0.1% PVP). Then, embryos were incubated overnight at 4 °C with mouse anti-OCT4 antibody (Santa Cruz, sc-5279) diluted with 1:200, rabbit anti-CDX2 antibody 1:200 (Abcam, ab76541), goat anti-GATA6 antibody 1:400 (R&D Systems, AF1700) and goat anti-NANOG antibody 1:200 (R&D Systems, AF1997). The next day, the embryos were washed three times with PBS containing 0.01% Tween-20 and 0.1% PVP and incubated in blocking buffer with anti-rabbit antibody (Thermo Fisher Scientific, A-21447), anti-mouse antibody (Thermo Fisher Scientific, A-31570) and anti-goat antibody (Thermo Fisher Scientific, A-31572) for 2 hours at room temperature. Nuclei were stained with DAPI for 30 minutes at room temperature. Finally, the stained embryos were washed with PBS containing 0.01% Tween-20 and 0.1% PVP three times (10 minutes each) before taking a picture under a microscope.

Microsatellite parentage analysis of genomic DNA employing short tandem repeat (STR)

DNA from the oocyte donor, sperm donor, surrogate, newborn monkey, and aESCs was extracted using the Wizard Genomic DNA Purification Kit (Promega, A1125) following the manufacturer's instructions. Total seventeen microsatellites (STRs: D2S102, D5S820, D6S2741, D6S311, D7S1827, D8S1106, D10S1432, D12S86, D13S765, D14S3306, D15S644, D16S415, D17S1290, D18S536, D19S255, D21S1256 and DXS8043) were selected to detect genotype of aESCs and infant. Locus-specific primers each containing a fluorescent dye (FAM/TAMRA/JOE) were used for PCR amplification in batches. The touchdown PCR conditions for each STR locus are set up (from 65 °C, down to 58 °C, and amplified 30 cycles at 58 °C). Amplification products were run on an ABI 3130XL sequencer following the manufacturer's recommendations, and the Liz 500 (Applied Biosystems, Foster City, CA) size standards were included to establish allele size. The results were analyzed by the software GeneMapper v4.0.

Bulk RNA sequencing (RNA-seq) and transcriptomic analysis

Total RNA was extracted from spESCs, ESCs, and hESCs using the TRIzol™ reagent (Thermo Fisher Scientific, 15596018) according to the manufacturer's instructions. Subsequently, an RNA library was generated using the NEBNext® Ultra RNA Library Prep Kit for Illumina® (NEB England BioLabs, E7530L), and sequencing was performed on the HiSeq X Ten platform. Raw reads were subjected to adaptor trimming and filtering of low-quality reads by fastp (v0.21.4)[69]. Qualified reads were mapped to the corresponding reference genome (Macaca_fascicularis_5.0 for Macaca fascicularis, and GRCh38 for Homo sapiens) using Hisat2 (v2.2.1)[70]. Gene expression was quantified from the refined BAM files using StringTie (v2.0.4)[71] and is reported as transcripts per

million (TPM). Integration and analysis of data from this study and published sources identified co-expressed genes across all cells[39]. Correlation heatmaps were plotted using pheatmap packages (version 1.0.12). Notes: one spESCs did not meet the quality control standards and was excluded from subsequent experiments.

scRNA-seq library preparation, sequencing, and pre-processing

After dissociating PSCs using IV collagenases, the cells were treated with TrypLE Express Enzyme to maintain a single-cell state. Subsequently, the cells were loaded onto the 10 × Genomics Chromium system and prepared for library construction following the manufacturer's instructions. The raw data were aligned to the *Macaca mulatta* reference genome (Mmul_10) and quantified using CellRanger software (Version 6.0.2). Genes expressed in fewer than three cells were excluded from the analysis. Additionally, doublet detection and removal were performed using the R packages DoubletFinder and Seurat. Subsequently, cells with gene count below 1800 and above 7500 were excluded, which may indicate low quality or non-single cells. For detailed quality control criteria, please refer to Supplementary Fig. 4. The downstream analysis, including data normalization, identification of highly variable genes (HVGs), dimensionality reduction, and clustering of cells was conducted utilizing the Seurat R packages (https://satijalab.org/seurat).

DEGs identification and cell cluster annotation

We determined the overlap between the expressed genes in all cell clusters and the known pluripotency genes[40,41]. Then, we computed the mean expression levels and cell expression proportions of the top 30 pluripotency genes in each cell cluster and visualized them by the "DotPlot" function of Seurat. Next, we integrated our data with scRNA-sequencing data from in vitro cynomolgus embryos[44] and in vivo CS7 human embryos[45], enabling the identification of Epi cells.

Correlation analysis between our scRNA-seq dataset and a Carnegie stage 7 (CS7) human gastrula dataset revealed that most cell clusters of PSCs grown in two different conditions maintained a pluripotent state without differentiation propensity (DPR)[45], which we annotated as "Epi". However, a few cell clusters may exhibit different DPR (Supplementary Fig. 5a, i). This prompted us to hypothesize that while these cell populations are PSCs, they might have initiated the expression of certain genes associated with differentiated cell types in the transcriptome. To test this hypothesis, we initially compared each cell cluster with Epi to analyze DEGs. The Seurat package's FindMarkers function was used to identify DEGs between each cell cluster (excluding Epi) and the Epi cell cluster, with a p-value < 0.05 as gene set A. Then, gene set B (Marker genes for each cluster) was identified by the "FindAllMarkers" function with the cutoff of p value < 0.05. The intersection of gene set A and gene set B was taken to obtain the collection of significant and specific DEGs for each cell cluster (Supplementary Fig. 5b and Supplementary Data 1). Using these DEGs in combination with known signature genes, five cell populations with different DPR were annotated in PSCs cultured on feeder layers, each highly expressing some specific genes (Supplementary Fig. 5b). Additionally, there is a cell population (cluster 10) that exhibits transcriptomic similarity to the defined Epi. Therefore, we evaluated these two cell populations based on known pluripotency genes and designated them as "Epi2" according to the scoring results (Supplementary Fig. 5c). In contrast, for the PSCs cultured on feeder-free layers, besides Epi cells, only ExE mech DPR was annotated, which expressed ExE mech specific genes such as *FN1*, *COL1A2*, *COL1A1*, and *TIMP3* (Supplementary Fig. 5k and Supplementary Data 2).

After excluding stem cells with DPR, we compared gene expression between iPSCs and aESCs, as well as ntESCs and aESCs. We identified the genes with p value < 0.05 and different FC thresholds (FC > 1 or <1 and FC ≥1.5 or ≤0.67) as DEGs.

Cell fate prediction

The FateID method uses an iterative random forest classification strategy to quantify bias towards specific cell fates in single-cell transcriptome datasets and calculate the pre-existing probability of each progenitor cell for one or more alternative terminal fates[46]. We integrate our single-cell transcriptomic data with published articles to identify cell differential biases using the integrated expression matrix and reference cells, including Meso[44,45], Endo[44,45], NNE[45], ExE mech[37,44], and NPCs[72]. After excluding the reference cell types, we compute each cell's fate bias using the FateID package and define cell types based on the probability values of the fate bias. The results further validate the cell-type annotation (Supplementary Fig. 5e–h, j).

Gene functional enrichment analyses for DEGs

The DEGs (p-value < 0.05 and FC > 1 or <1) were subjected to gene functional enrichment analysis using clusterProfiler (v4.0.2)[73] based on the Gene Ontology (GO) and Kyoto Encyclopedia of Genes and Genomes (KEGG) pathways. Then, we calculated the proportion of up- and down-regulated genes enriched in each term and used ggplot2 (v3.4.3) to visualize the results.

Gene expression scoring for the gene sets associated with genomic instability

The gene sets mentioned in the previous work were used to evaluate the genomic instability of the Epi cells in the three types of PSCs using the Addmodulescore function of the Seurat package[47]. To compare genomic stability differences among the Epi cells in the three types of PSCs, we conducted a rank-sum test using the wilcox_test function from rstatix package (v0.7.2) and adjusted the p-value for multiple testing using the false discovery rate (FDR) method.

Copy number variation inference

The initial CNVs for each Epi cell from each type of PSCs were estimated using the inferCNV package of R (version 1.8.1)[74]. The CNV matrix was calculated using the 'run' function, where each value in the CNV matrix is adjusted by subtracting one to represent the CNV score for each cell. The CNV level of each cell is defined as the mean of the absolute values of the CNV scores for all genes within that cell. Differences in CNV levels of Epi cells among the three types of PSCs were compared using the rank-sum test via wilcox_test function, with the p-values adjusted using the FDR method.

Estimation of transcriptional noise

The methodology described in previous work was used to quantify transcriptional noise in the gene expression[48]. First, all cells were downsampled to have equal total UMI counts. Then, the number of cells was further downsampled to ensure an equal number of Epi cells from each type of PSCs for subsequent comparative calculations. Next, the genes were categorized into 10 equally sized bins according to their mean expression levels, excluding the first and last bins. The genes with the lowest 10% coefficient of variation in each bin were selected as the minimal fluctuation gene set. Based on this gene set, the downsampled raw count matrix was subsetted and subjected to square root transformation. Next, the Euclidean distance between the expression of each cell and the average expression of all cells within the same types of PSCs was calculated as a measure of transcriptional noise for each cell. To statistically evaluate the differences in transcriptional noise among different types of PSCs in the Epi cells, we performed a rank-sum test using the wilcox_test function and adjusted the p-values for multiple testing using the FDR method.

We also performed functional enrichment analysis on the minimal fluctuation gene set using clusterProfiler (v4.0.2)[73]. Additionally, pairwise rank-sum tests were conducted on the top 100 genes with minimal changes to assess transcriptional noise differences among Epi cells from three types of PSCs.

Statistics and reproducibility

The statistical differences in Fig. 1g (cynomolgus monkey 2/4th embryos, n = 176; identical pairs, n = 56; controls, n = 169), Fig. 1h (cynomolgus monkey 3/8th and 5/8th embryos, n = 92; identical pairs, n = 40; controls, n = 53), Fig. 1k (controls, n = 13; 2/4th embryos, n = 18, 9 pairs; 3/8th embryos and 5/8th embryos, n = 18, 9 pairs), Supplementary Fig. 1e (rhesus monkey 2/4th embryos, n = 72; identical pairs, n = 22; controls, n = 77), Supplementary Fig. 1f (rhesus monkey 3/8th and 5/8th embryos, n = 70; identical pairs, n = 42; controls, n = 44), Fig. 2b (2/4th blastocysts, n = 25, 3/8th blastocysts, n = 26; controls, n = 45), Fig. 2c (3/8th blastocysts, n = 26; controls, n = 45), 7c-e (split embryos, n = 5; controls, n = 3), and Supplementary Fig. 7f (split embryos, n = 5; controls, n = 3) were analyzed by unpaired two-tailed Student's t-test. The statistical differences in Fig. 1i (2/4th embryos, n = 18, 9 pairs; controls, n = 13), Fig. 1j (3/8th embryos and 5/8th embryos, n = 18, 9 pairs; controls, n = 13), and Supplementary Fig. 1i–l (controls, n = 13, 2/4th embryos, n = 18, 9 pairs; 3/8th embryos and 5/8th embryos, n = 18, 9 pairs) were analyzed by paired two-tailed Student's t-test. Multiple t-tests were used to analyze the weight and body length comparison between split embryos (n = 5) and controls (n = 5) shown in Fig. 3c, d. GraphPad Prism 6 software was used for analyzing data. The statistical differences in Fig. 6j, k, Supplementary Fig. 5c, and 6c were analyzed with the unpaired Wilcoxon test function from the rstatix package in R (version: 0.7.2), while Supplementary Fig. 6d was analyzed with the paired Wilcoxon test. Source data are provided with this paper.

Reporting summary

Further information on research design is available in the Nature Portfolio Reporting Summary linked to this article.

Data availability

The raw data generated in this study have been deposited in the Genome Sequence Archive[75] in National Genomics Data Center[76], China National Center for Bioinformation / Beijing Institute of Genomics, Chinese Academy of Sciences database under accession code CRA013609 and HRA006090. Source data are provided with this paper.

References

1. McKay, R. Stem cells–hype and hope. *Nature* **406**, 361–364 (2000).
2. Yamanaka, S. Pluripotent stem cell-based cell therapy-promise and challenges. *Cell Stem Cell* **27**, 523–531 (2020).
3. Du, Y. et al. Human pluripotent stem-cell-derived islets ameliorate diabetes in non-human primates. *Nat. Med* **28**, 272–282 (2022).
4. Mandai, M. et al. Autologous induced stem-cell-derived retinal cells for macular degeneration. *N. Engl. J. Med* **376**, 1038–1046 (2017).
5. Tachibana, M. et al. Human embryonic stem cells derived by somatic cell nuclear transfer. *Cell* **153**, 1228–1238 (2013).
6. Ruiz, S. et al. Analysis of protein-coding mutations in hiPSCs and their possible role during somatic cell reprogramming. *Nat. Commun.* **4**, 1382 (2013).
7. Ma, H. et al. Abnormalities in human pluripotent cells due to reprogramming mechanisms. *Nature* **511**, 177–183 (2014).
8. Edwards, M. M., N. Wang, D. J. Massey, D. Egli & A. Koren. Incomplete reprogramming of DNA replication timing in induced pluripotent stem cells. *Cell Rep.* **43**, 113664 (2024).
9. Matoba, S. & Zhang, Y. Somatic cell nuclear transfer reprogramming: mechanisms and applications. *Cell Stem Cell* **23**, 471–485 (2018).
10. Byrne, J. A. et al. Producing primate embryonic stem cells by somatic cell nuclear transfer. *Nature* **450**, 497–502 (2007).
11. Willadsen, S. M. A method for culture of micromanipulated sheep embryos and its use to produce monozygotic twins. *Nature* **277**, 298–300 (1979).
12. Allen, W. R. & Pashen, R. L. Production of monozygotic (identical) horse twins by embryo micromanipulation. *J. Reprod. Fertil.* **71**, 607–613 (1984).
13. Tsunoda, Y., Tokunaga, T., Sugie, T. & Katsumata, M. Production of monozygotic twins following the transfer of bisected embryos in the goats. *Theriogenology* **24**, 337–343 (1985).
14. Reichelt, B. & Niemann, H. Generation of identical twin piglets following bisection of embryos at the morula and blastocyst stage. *J. Reprod. Fertil.* **100**, 163–172 (1994).
15. Tagawa, M. et al. Production of monozygotic twin calves using the blastomere separation technique and Well of the Well culture system. *Theriogenology* **69**, 574–582 (2008).
16. Chan, A. W. et al. Clonal propagation of primate offspring by embryo splitting. *Science* **287**, 317–319 (2000).
17. Mitalipov, S. M., Yeoman, R. R., Kuo, H. C. & Wolf, D. P. Monozygotic twinning in rhesus monkeys by manipulation of in vitro-derived embryos. *Biol. Reprod.* **66**, 1449–1455 (2002).
18. Schramm, R. D. & Paprocki, A. M. In vitro development and cell allocation following aggregation of split embryos with tetraploid or developmentally asynchronous blastomeres in rhesus monkeys. *Cloning Stem Cells* **6**, 302–314 (2004).
19. Van de Velde, H., Cauffman, G., Tournaye, H., Devroey, P. & Liebaers, I. The four blastomeres of a 4-cell stage human embryo are able to develop individually into blastocysts with inner cell mass and trophectoderm. *Hum. Reprod.* **23**, 1742–1747 (2008).
20. Illmensee, K., Levanduski, M., Vidali, A., Husami, N. & Goudas, V. T. Human embryo twinning with applications in reproductive medicine. *Fertil. Steril.* **93**, 423–427 (2010).
21. Noli, L. et al. Developmental clock compromises human twin model created by embryo splitting. *Hum. Reprod.* **30**, 2774–2784 (2015).
22. Noli, L., Ogilvie, C., Khalaf, Y. & Ilic, D. Potential of human twin embryos generated by embryo splitting in assisted reproduction and research. *Hum. Reprod. Update* **23**, 156–165 (2017).
23. Klimanskaya, I., Chung, Y., Becker, S., Lu, S. J. & Lanza, R. Human embryonic stem cell lines derived from single blastomeres. *Nature* **444**, 481–485 (2006).
24. Chung, Y. et al. Human embryonic stem cell lines generated without embryo destruction. *Cell Stem Cell* **2**, 113–117 (2008).
25. Yang, J. et al. Establishment of mouse expanded potential stem cells. *Nature* **550**, 393–397 (2017).
26. Chung, Y. et al. Embryonic and extraembryonic stem cell lines derived from single mouse blastomeres. *Nature* **439**, 216–219 (2006).
27. Simpson, J. L. Blastomeres and stem cells. *Nature* **444**, 432–435 (2006).
28. Takashima, Y. et al. Resetting transcription factor control circuitry toward ground-state pluripotency in human. *Cell* **158**, 1254–1269 (2014).
29. Gao, X. et al. Establishment of porcine and human expanded potential stem cells. *Nat. Cell Biol.* **21**, 687–699 (2019).
30. Ai, Z. et al. Modulation of Wnt and activin/nodal supports efficient derivation, cloning and suspension expansion of human pluripotent stem cells. *Biomaterials* **249**, 120015 (2020).
31. Irie, N. et al. SOX17 is a critical specifier of human primordial germ cell fate. *Cell* **160**, 253–268 (2015).
32. Morris, S. A., Guo, Y. & Zernicka-Goetz, M. Developmental plasticity is bound by pluripotency and the Fgf and Wnt signaling pathways. *Cell Rep.* **2**, 756–765 (2012).
33. Torres-Padilla, M. E., Parfitt, D. E., Kouzarides, T. & Zernicka-Goetz, M. Histone arginine methylation regulates pluripotency in the early mouse embryo. *Nature* **445**, 214–218 (2007).
34. Goolam, M. et al. Heterogeneity in Oct4 and Sox2 targets biases cell fate in 4-cell mouse embryos. *Cell* **165**, 61–74 (2016).
35. White, M. D. et al. Long-lived binding of Sox2 to DNA predicts cell fate in the four-cell mouse embryo. *Cell* **165**, 75–87 (2016).

36. Casser, E. et al. Differences in blastomere totipotency in 2-cell mouse embryos are a maternal trait mediated by asymmetric mRNA distribution. *Mol. Hum. Reprod.* **25**, 729–744 (2019).
37. Niu, Y. et al. Dissecting primate early post-implantation development using long-term in vitro embryo culture. *Science* **366**, eaaw5754 (2019).
38. Wu, J. et al. Long-term in vivo chimeric cells tracking in non-human primate. *Protein Cell* **15**, 207–222 (2023).
39. Chen, Y. et al. Generation of cynomolgus monkey chimeric fetuses using embryonic stem cells. *Cell Stem Cell* **17**, 116–124 (2015).
40. Liu, D. et al. Single-cell RNA-sequencing reveals the existence of naive and primed pluripotency in pre-implantation rhesus monkey embryos. *Genome Res* **28**, 1481–1493 (2018).
41. Neagu, A. et al. In vitro capture and characterization of embryonic rosette-stage pluripotency between naive and primed states. *Nat. Cell Biol.* **22**, 534–545 (2020).
42. Tachibana, M. et al. Generation of chimeric rhesus monkeys. *Cell* **148**, 285–295 (2012).
43. Liu, Z. et al. Cloning of macaque monkeys by somatic cell nuclear transfer. *Cell* **172**, 881–887.e7 (2018).
44. Yang, R. et al. Amnion signals are essential for mesoderm formation in primates. *Nat. Commun.* **12**, 5126 (2021).
45. Tyser, R. C. V. et al. Single-cell transcriptomic characterization of a gastrulating human embryo. *Nature* **600**, 285–289 (2021).
46. Herman, J. S., Sagar & Grun, D. FateID infers cell fate bias in multipotent progenitors from single-cell RNA-seq data. *Nat. Methods* **15**, 379–386 (2018).
47. Aguilera, A. & Gómez-González, B. Genome instability: a mechanistic view of its causes and consequences. *Nat. Rev. Genet.* **9**, 204–217 (2008).
48. Enge, M. et al. Single-cell analysis of human pancreas reveals transcriptional signatures of aging and somatic mutation patterns. *Cell* **171**, 321–330.e14 (2017).
49. Angelidis, I. et al. An atlas of the aging lung mapped by single cell transcriptomics and deep tissue proteomics. *Nat. Commun.* **10**, 963 (2019).
50. Mohammed, H. et al. Single-cell landscape of transcriptional heterogeneity and cell fate decisions during mouse early gastrulation. *Cell Rep.* **20**, 1215–1228 (2017).
51. Gerri, C. et al. Initiation of a conserved trophectoderm program in human, cow and mouse embryos. *Nature* **587**, 443–447 (2020).
52. Chin, M. H. et al. Induced pluripotent stem cells and embryonic stem cells are distinguished by gene expression signatures. *Cell Stem Cell* **5**, 111–123 (2009).
53. Bock, C. et al. Reference Maps of human ES and iPS cell variation enable high-throughput characterization of pluripotent cell lines. *Cell* **144**, 439–452 (2011).
54. Choi, J. et al. A comparison of genetically matched cell lines reveals the equivalence of human iPSCs and ESCs. *Nat. Biotechnol.* **33**, 1173–1181 (2015).
55. Zhao, M. T. et al. Molecular and functional resemblance of differentiated cells derived from isogenic human iPSCs and SCNT-derived ESCs. *Proc. Natl. Acad. Sci. USA* **114**, E11111–E11120 (2017).
56. Rouhani, F. et al. Genetic background drives transcriptional variation in human induced pluripotent stem cells. *PLoS Genet.* **10**, e1004432 (2014).
57. Kilpinen, H. et al. Common genetic variation drives molecular heterogeneity in human iPSCs. *Nature* **546**, 370–375 (2017).
58. Stadtfeld, M. et al. Aberrant silencing of imprinted genes on chromosome 12qF1 in mouse induced pluripotent stem cells. *Nature* **465**, 175–181 (2010).
59. Kim, K. et al. Donor cell type can influence the epigenome and differentiation potential of human induced pluripotent stem cells. *Nat. Biotechnol.* **29**, 1117–1119 (2011).
60. Kang, Y. et al. Improving cell survival in injected embryos allows primed pluripotent stem cells to generate chimeric cynomolgus monkeys. *Cell Rep.* **25**, 2563–2576.e9 (2018).
61. Mallon, B. S. et al. Comparison of the molecular profiles of human embryonic and induced pluripotent stem cells of isogenic origin. *Stem Cell Res.* **12**, 376–386 (2014).
62. Yu, L. et al. Core pluripotency factors promote glycolysis of human embryonic stem cells by activating GLUT1 enhancer. *Protein Cell* **10**, 668–680 (2019).
63. Shen, F., Song, C., Liu, Y., Zhang, J. & Wei Song, S. IGFBP2 promotes neural stem cell maintenance and proliferation differentially associated with glioblastoma subtypes. *Brain Res.* **1704**, 174–186 (2019).
64. Zhao, Q. et al. BNIP3-dependent mitophagy safeguards ESC genomic integrity via preventing oxidative stress-induced DNA damage and protecting homologous recombination. *Cell Death Dis.* **13**, 976 (2022).
65. Piotrowska-Nitsche, K., Perea-Gomez, A., Haraguchi, S. & Zernicka-Goetz, M. Four-cell stage mouse blastomeres have different developmental properties. *Development* **132**, 479–490 (2005).
66. Nolte, T. et al. Animal and vegetal materials of mouse oocytes segregate at first zygotic cleavage: a simple mechanism that makes the two-cell blastomeres differ reciprocally from the start. *Mol Hum Reprod* **31**, gaae045 (2025).
67. Ma, H. et al. In vitro culture of cynomolgus monkey embryos beyond early gastrulation. *Science* **366**, eaax7890 (2019).
68. Liu, B. et al. Chemically defined and xeno-free culture condition for human extended pluripotent stem cells. *Nat. Commun.* **12**, 3017 (2021).
69. Chen, S., Zhou, Y., Chen, Y. & Gu, J. fastp: an ultra-fast all-in-one FASTQ preprocessor. *Bioinformatics* **34**, i884–i890 (2018).
70. Kim, D., Paggi, J. M., Park, C., Bennett, C. & Salzberg, S. L. Graph-based genome alignment and genotyping with HISAT2 and HISAT-genotype. *Nat. Biotechnol.* **37**, 907–915 (2019).
71. Pertea, M. et al. StringTie enables improved reconstruction of a transcriptome from RNA-seq reads. *Nat. Biotechnol.* **33**, 290–295 (2015).
72. Zhong, S. et al. A single-cell RNA-seq survey of the developmental landscape of the human prefrontal cortex. *Nature* **555**, 524–528 (2018).
73. Yu, G., Wang, L. G., Han, Y. & He, Q. Y. clusterProfiler: an R package for comparing biological themes among gene clusters. *Omics* **16**, 284–287 (2012).
74. Patel, A. P. et al. Single-cell RNA-seq highlights intratumoral heterogeneity in primary glioblastoma. *Science* **344**, 1396–1401 (2014).
75. Chen, T. et al. The genome sequence archive family: toward explosive data growth and diverse data types. *Genomics Proteom. Bioinformatics* **19**, 578–583 (2021).
76. Database Resources of the National Genomics Data Center, China National Center for Bioinformation in 2022. *Nucleic Acids Res.* **50**, D27-d38 (2022).
77. Liu, X. et al. Function of FEZF1 during early neural differentiation of human embryonic stem cells. *Sci. China Life Sci.* **61**, 35–45 (2018).
78. Guo, C. et al. Fezf2 expression identifies a multipotent progenitor for neocortical projection neurons, astrocytes, and oligodendrocytes. *Neuron* **80**, 1167–1174 (2013).
79. Hou, P. S. et al. LHX2 regulates the neural differentiation of human embryonic stem cells via transcriptional modulation of PAX6 and CER1. *Nucleic Acids Res.* **41**, 7753–7770 (2013).
80. Scott, C. E. et al. SOX9 induces and maintains neural stem cells. *Nat. Neurosci.* **13**, 1181–1189 (2010).
81. Sandberg, M., Kallstrom, M. & Muhr, J. Sox21 promotes the progression of vertebrate neurogenesis. *Nat. Neurosci.* **8**, 995–1001 (2005).

82. Whittington, N., Cunningham, D., Le, T. K., De Maria, D. & Silva, E. M. Sox21 regulates the progression of neuronal differentiation in a dose-dependent manner. *Dev. Biol.* **397**, 237–247 (2015).
83. Ross, C. & Boroviak, T. E. Origin and function of the yolk sac in primate embryogenesis. *Nat. Commun.* **11**, 3760 (2020).
84. Nakamura, T. et al. A developmental coordinate of pluripotency among mice, monkeys and humans. *Nature* **537**, 57–62 (2016).

Acknowledgements

This work was supported by grants from the National Key R&D Program of China (2021YFA0805700 to Y.N. and 2021YFA1102000 to Y.K.), the National Natural Science Foundation of China (32460179 to C.S., U2102204 to Y.N. and 32160153 to S.D.), the Natural Science Foundation of Yunnan Province (202102AA100053 to W.J. and 202105AD160008 to S.D.), and the Key Projects of Yunnan Province Science and Technology Department (202302AA310044 to L.X.). Special thanks are due to Laboratory Animal Center of Institute of Primate Translational Medicine, Kunming University of Science and Technology, for animal feeding management and experimental operation. We thank Yandong Gong from state key laboratory of experimental hematology for help in bioinformatics analysis.

Author contributions

Y.N., S.D. and W.J. designed the study and supervised all experiments. C.S. performed construction of split embryo, embryo transplantation and embryo immunofluorescent staining. J.W., Z.C., S.Y., Z.T., Z.Y.L and J.Z. performed stem cell isolation, culture and identification. R.Z., C.S., P.Y., and S.D. performed bioinformatics analysis. Y.K. performed the somatic cell nuclear transfer procedure. C.C. performed the library construction of PSCs. Y.P. and Z.Y. performed STR analysis. L.X. performed human embryo culture. X.C., B.T. and Z.L. performed superovulation and animal care. C.S., S.D., W.J., and Y.N. wrote the manuscript, with contributions from all authors.

Competing interests

We declare that we have a patent application related to this manuscript. The patent titled “Methods for producing autologous embryonic stem cells in non-human primates through embryo splitting” is held by Kunming University of Science and Technology. The inventors listed are Y.N., C.S., and J.W. The application number is 202410668256.3, filed on May 28th, 2024, and has been granted. This patent specifically covers the methods described in the manuscript for establishing autologous embryonic stem cells (ESCs) via embryo splitting in non-human primates. All other authors declare no competing interests.

Additional information

Supplementary information The online version contains supplementary material available at https://doi.org/10.1038/s41467-025-60694-5.

Correspondence and requests for materials should be addressed to Weizhi Ji, Shaoxing Dai or Yuyu Niu.

Peer review information *Nature Communications* thanks Duanqing Pei, and the other, anonymous, reviewer(s) for their contribution to the peer review of this work. A peer review file is available.